NASA TECHNICAL MEMORANDUM

NASA TM X-2069

NASA TM X-2069

REAL-TIME DIGITAL-COMPUTER-HARDWARE SIMULATION OF A SPACECRAFT WITH CONTROL-MOMENT-GYROSCOPE STABILIZATION

by Claude R. Keckler, Robert G. Kyle, Ralph W. Will, and Charles T. Woolley

Langley Research Center
Hampton, Va. 23365

NATIONAL AERONAUTICS AND SPACE ADMINISTRATION • WASHINGTON, D. C. • SEPTEMBER 1970

1. Report No.	2. Government Accession No.	3. Recipient's Catalog No.
NASA TM X-2069		

4. Title and Subtitle	5. Report Date
REAL-TIME DIGITAL-COMPUTER-HARDWARE SIMULATION OF A SPACECRAFT WITH CONTROL-MOMENT-GYROSCOPE STABILIZATION	September 1970
	6. Performing Organization Code

7. Author(s)	8. Performing Organization Report No.
Claude R. Keckler, Robert G. Kyle, Ralph W. Will, and Charles T. Woolley	L-6555
	10. Work Unit No.
	965-21-00-01
9. Performing Organization Name and Address	11. Contract or Grant No.
NASA Langley Research Center Hampton, Va. 23365	
	13. Type of Report and Period Covered
12. Sponsoring Agency Name and Address	Technical Memorandum
National Aeronautics and Space Administration Washington, D.C. 20546	14. Sponsoring Agency Code

15. Supplementary Notes

16. Abstract

A description of a real-time digital-computer-hardware simulation of an Apollo-Telescope-Mount (ATM) mission is presented. The simulation has been employed to evaluate the performance of a full-scale control-moment-gyroscope (CMG) system in providing stabilization for the ATM cluster.

For this evaluation, a full-scale CMG system is linked to a real-time digital-computer program representing the ATM cluster. This program consists of the spacecraft rigid- and flexible-body dynamics, internal and external disturbances, and the baseline CMG system momentum-feedback control law with isogonal correction.

System-stability and limit-cycling problems were encountered during initial operations. These problems are discussed and possible solutions are outlined.

17. Key Words (Suggested by Author(s))	18. Distribution Statement
Control-moment gyroscope Stabilization	Unclassified – Unlimited

19. Security Classif. (of this report)	20. Security Classif. (of this page)	21. No. of Pages	22. Price*
Unclassified	Unclassified	51	$3.00

*For sale by the Clearinghouse for Federal Scientific and Technical Information
Springfield, Virginia 22151

REAL-TIME DIGITAL-COMPUTER-HARDWARE SIMULATION OF A SPACECRAFT WITH CONTROL-MOMENT-GYROSCOPE STABILIZATION

By Claude R. Keckler, Robert G. Kyle, Ralph W. Will,
and Charles T. Woolley
Langley Research Center

SUMMARY

A description of a real-time digital-computer-hardware simulation of an Apollo-Telescope-Mount (ATM) mission is presented. The simulation has been employed to evaluate the performance of a full-scale control-moment-gyroscope (CMG) system in providing stabilization for the ATM cluster.

For this evaluation, a full-scale CMG system is linked to a real-time digital-computer program representing the ATM cluster. This program consists of the spacecraft rigid- and flexible-body dynamics, internal and external disturbances, and the baseline CMG system momentum-feedback control law with isogonal correction.

System-stability and limit-cycling problems were encountered during initial operations. These problems are discussed and possible solutions are outlined.

INTRODUCTION

Theoretical research on the feasibility of using control-moment gyroscopes (CMG's) as the primary attitude-control system for long-term manned missions has indicated that CMG's offer significant advantages over other more conventional control concepts.

The CMG is a double-gimbal device, which introduces torques by the precession of a constant-speed inertia wheel. A control system employing CMG's is capable of providing the wide torque range necessary for performing all of the control tasks, such as maneuvering and fine pointing, required for long-term manned missions, such as the Apollo Telescope Mount (ATM). Furthermore, a CMG control system minimizes the optics-contaminant problems of reaction-jet systems, since CMG momentum dumping can be accomplished through gravity-gradient desaturation as shown by information obtained from H. F. Kennel at the Marshall Space Flight Center. Because of their unique

characteristics, CMG systems also offer significant weight savings for long-term missions over conventional control systems.

To verify the results from preliminary CMG research, a real-time digital-computer simulation of the ATM vehicle was developed. In the course of the CMG developmental research, several analog-computer simulations have been developed and utilized effectively. The problem of simulating the complete ATM mission is much larger and more complex than any of the preceding simulations. Because of many algebraic computations, a large dynamic range, and high resolution, digital computation was required. Hardware complexities and nonlinearities of the CMG system make a complete and realistic simulation of this hardware extremely difficult. Accurate representation of the CMG system characteristics is best provided by including the hardware in the simulation. This inclusion imposes the requirement of real-time operation. The first such real-time simulation employing a digital computer linked to a full-scale CMG control system has been developed and successfully utilized at the Langley Research Center for the Marshall Space Flight Center ATM mission.

The general objectives of the static test program at the Langley Research Center were (1) to determine the CMG hardware characteristics, (2) to evaluate the hardware in the spacecraft control loop, and (3) to refine the response characteristics of the CMG system.

This report presents a detailed description of the simulation used in the static test program in the form of flow charts, equations, hardware description, and discussions of simulation and system problems and solutions.

SYMBOLS AND ABBREVIATIONS

Symbols

BE	intermediate quantities defined by equations (34)
$[E]$	3×3 direction-cosine input matrix to isogonal correction law
E'	modified direction cosine
E_T	isogonal total CMG momentum component, lbf-ft-sec (N-m-sec)
e_I	error of the isogonal distribution law
e_r	error of the rotation law

F_A crew-motion-disturbance force applied at ATM crew location, lbf (newtons)

F_J crew-motion-disturbance force applied at CSM crew location, lbf (newtons)

F_W crew-motion-disturbance force applied at S-IVB crew location, lbf (newtons)

$\{G\}$ control-torque components of CMG system, lbf-ft (N-m)

$\{GE\}$ total generalized disturbance applied to flexible body, lbf-ft; lbf (N-m; newtons)

H individual CMG momentum magnitude, lbf-ft-sec (N-m-sec)

$\{H_c\}$ command-momentum components, lbf-ft-sec (N-m-sec)

$\{H_e\}$ momentum-error components, lbf-ft-sec (N-m-sec)

H_x, H_y, H_z momentum components of CMG system, lbf-ft-sec (N-m-sec)

$[I]$ 96×96 total-body generalized inertia-mass matrix, lbf-ft-sec^2 (N-m-sec^2)

I_{xx}, I_{yy}, I_{zz} principal moments of inertia of body, slug-ft^2 (kg-m2)

J inertia, lbf-ft-sec^2 (N-m-sec^2)

$[K]$ 96×96 total-body generalized stiffness matrix, lbf-ft/rad (N-m/rad)

K_a gain of gimbal-angle filter compensation, seconds

K_D, K_{DP} actual and nominal isogonal distribution-law gains, rad/lbf-ft-sec^2 (rad/N-m-sec^2)

K_r rotation-law gain for isogonal correction law, lbf-ft (N-m)

K_{SL} effective inner-loop gain, rad/lbf-ft-sec^2 (rad/N-m-sec^2)

$K_{SL_\alpha}, K_{SL_\beta}$ steering-law gains for outer and inner gimbal of CMG, rad/lbf-ft-sec^2 (rad/N-m-sec^2)

K_ϕ, K_θ, K_ψ proportional torque-command-attitude gains of CMG system, lbf-ft/rad (N-m/rad)

$K_{\dot{\phi}}, K_{\dot{\theta}}, K_{\dot{\psi}}$ proportional torque-command-rate gains of CMG system, lbf-ft/rad/sec (N-m/rad/sec)

L_A distance of application of ATM crew-motion disturbance from cluster center of gravity, feet (meters)

L_J distance of application of CSM crew-motion disturbance from cluster center of gravity, feet (meters)

L_W distance of application of S-IVB crew-motion disturbance from cluster center of gravity, feet (meters)

M_A crew-motion-disturbance moment applied at ATM crew location, lbf-ft (N-m)

M_f filtered command moment component, lbf-ft (N-m)

M_J crew-motion-disturbance moment applied at CSM crew location, lbf-ft (N-m)

M_W crew-motion-disturbance moment applied at S-IVB crew location, lbf-ft (N-m)

$\{M_c\}$ command-moment components of CMG system, lbf-ft (N-m)

$\{M_\epsilon\}$ total external-disturbance moment components, lbf-ft (N-m)

$\{M_\iota\}$ total internal-disturbance moment components, lbf-ft (N-m)

$\{N\}$ 96 generalized normal coordinates

$\{\dot{N}\}$ 96 generalized normal rates, rad/sec

$\{\ddot{N}\}$ 96 generalized normal accelerations, rad/sec^2

$[P]$ 3×7 modal-participation matrix

q determinant of $[E]$

R intermediate quantities defined by equations (38)

s	Laplace transform
$\{T_R\}$	total torque applied to rigid body, lbf-ft (N-m)
t	time, seconds
$[U]$	7×18 modal-distribution matrix
X,Y,Z	spacecraft axes
X_i,Y_i,Z_i	inertial reference axes
$\{x\}$	96 spatial coordinates
$\{\ddot{x}\}$	96 spatial accelerations, rad/sec^2
Z_O	orbit reference axis
α	CMG outer-gimbal angles, degrees
$\dot{\alpha}$	CMG outer-gimbal rates, deg/sec
$\dot{\alpha}_c$	continuous CMG outer-gimbal-rate commands, deg/sec
$\dot{\alpha}_{CI}$	periodic isogonal correction for outer-gimbal-rate commands, deg/sec
β	CMG inner-gimbal angles, degrees
$\dot{\beta}$	CMG inner-gimbal rates, deg/sec
$\dot{\beta}_c$	continuous CMG inner-gimbal-rate commands, deg/sec
$\dot{\beta}_{CI}$	periodic isogonal correction for inner-gimbal-rate commands, deg/sec
$\{\delta\}$	flexible-body attitude angles, radians
η	inertial to orbital reference angle, radians (see fig. 6)
λ	distribution-law gain

ξ	inertial to body reference angle, radians (see fig. 6)
ρ_f	bending-filter damping coefficient
σ	angle between orbit plane and sunline, radians (see fig. 6)
$[\Phi]$	96×96 modal-participation matrix
ϕ,θ,ψ	total-body modified Euler angles, radians
ϕ_c,θ_c,ψ_c	commanded-body modified Euler angles, radians
ϕ_F,θ_F,ψ_F	flexible-body modified Euler angles, radians
ϕ_R,θ_R,ψ_R	rigid-body modified Euler angles, radians
$\dot{\phi}_R,\dot{\theta}_R,\dot{\psi}_R$	rigid-body modified Euler rates, rad/sec
$\{\Omega\}$	total-body angular rates, rad/sec
Ω_c	commanded-body angular rates, rad/sec
$\{\Omega_F\}$	flexible-body angular rates, rad/sec
Ω_O	orbit rate, rad/sec
$\{\Omega_R\}$	rigid-body angular rates, rad/sec
$\dot{\Omega}_R$	rigid-body angular accelerations, rad/sec^2
$\begin{bmatrix} \omega^2 \end{bmatrix}$	96×96 modal-frequencies matrix, rad/sec
ω_f	bending-filter cutoff frequency, rad/sec

Subscripts:

x,y,z	components along spacecraft axes
1,2,3	individual CMG in system

n integer

A $[\,]^T$ denotes a transpose matrix.

Abbreviations

ATM	Apollo Telescope Mount
ADC	analog-to-digital converter
CMG	control-moment gyroscope
CSM	command and service module
DAC	digital-to-analog converter
LM	lunar module
MDA	multiple docking adapter
MSFC	George C. Marshall Space Flight Center
S-IVB	fourth stage of Saturn V launch vehicle

SIMULATION CONCEPT

Theoretical analyses of CMG systems have proven that these systems are capable of performing all the control tasks required by extended manned missions. (See ref. 1.) However, because of the inherent nonlinearities of CMG hardware as well as the complexity and inadequacy of CMG math models, these analyses have been limited to the assumptions of idealized characteristics for the CMG control-system hardware. To evaluate the impact of the nonlinear characteristics of the hardware on the control capability of the systems, a simulation of a typical manned spacecraft application was developed and linked to a full-scale CMG system. The ATM cluster, shown in figure 1, was chosen as being representative of all near-future manned spacecraft.

The ATM cluster consists of a repressurized S-IVB booster with a multiple docking adapter, an Apollo command and service module, and a modified lunar module. A gimbaled telescope experiment package is mounted in a rack attached to the LM. Three-axis spacecraft pointing to approximately 0.1° and 1 arc min/sec is required to support this experiment.

Analog simulations involving CMG systems have been evaluated but were found to be inadequate because of the large dynamic-range and resolution requirements associated with the ATM problem. Also, because of the complexity of the complete ATM simulation, a large number of algebraic computations were necessary which are not effectively performed on analog equipment. Therefore, it was apparent that a digital simulation was needed to meet these requirements; and since the simulation would be utilized in conjunction with CMG hardware, it must operate in real time. Digital hardware, while capable of efficient algebraic computation and high accuracy, is not as efficient as analog hardware in performing integrations. It thus became necessary to find an efficient and fast integration algorithm to meet the accuracy requirements of the ATM problem and still be compatible with real-time operation. In addition, the iteration interval required to provide a proper representation of the frequencies of the spacecraft and control system had to be established. A non-real-time digital program with a variable computing interval was developed and utilized to establish these parameters.

Preliminary-response and accuracy analyses using the non-real-time program indicated that a fourth-order Runge-Kutta integration of the spacecraft and control-system equations with an iteration interval of 0.0312 second was required for proper frequency representations. Since the CMG hardware is restricted in frequency to 2.5 hertz (1 hertz = 1 cps), the 0.0312 second computing interval allows 13 samples in the period of the highest frequency content and is sufficient to accurately represent the system response. A typical iteration frame is shown in figure 2. As can be observed, only 0.015 second is required to actually perform the computations; however, to meet real-time computer time-sharing requirements, a 0.0312-second interval is used. At the beginning of the computation interval, CMG gimbal rate and position information from the hardware are read into the program, and the integration step is initiated. At the end of each computation interval, the control-law commands are updated and transmitted to the CMG hardware.

The ATM cluster is represented by seven primary modes of flexibility. Spacecraft rate and attitude output of the computer program represent motions of the ATM module which houses the telescope. All body-angular-rate and attitude sensors are assumed linear and their outputs are represented by the rate and attitude outputs of the digital program. The control law used in the simulation represents the baseline CMG flight system, that is, the momentum-feedback concept (ref. 2) with isogonal correction (developed by H. F. Kennel at MSFC).

The simulation equations were programed in Fortran IV language on a Control Data series 6000 computer. This program is linked to the full-scale CMG system by trunk lines and by 14-bit plus sign-conversion equipment. (See fig. 3.) Simulation scaling is also shown in figure 3.

SIMULATION DESCRIPTION

A block diagram of the simulation is presented in figure 4. The digital program includes control and disturbance torques, rigid-body dynamics, vehicle flexibility, and the CMG system control law. The simulation can be divided into two major parts: the outer or vehicle loop and the inner or momentum-feedback loop, which is indicated by heavy lines in figure 4. The control torque generated by the CMG's and external- and internal-disturbance torques are summed, and this result is used as an input to the spacecraft rigid-body equations. The output of this computation is the rigid-body contribution to the body-attitude and angular rate errors. In addition, the CMG control torques and internal disturbances are used to determine the rate and attitude errors caused by the spacecraft flexibility. The external-disturbance torque is considered to be distributed over the entire vehicle, and the frequency is low enough so as not to excite the flexibility modes of the spacecraft. Therefore, the flexibility contribution to the spacecraft errors resulting from the external torques is neglected. The sum of the flexibility- and rigid-body-rate and attitude errors is used as spacecraft-sensor-output signals, since these sensors were assumed to be linear. By using these output signals, a required or command torque to correct for the spacecraft errors is generated. This command torque is passed through fourth-order bending filters to remove the higher frequency content. This procedure is necessary since the CMG system, because of its limited bandpass, would not respond properly to the high-frequency commands and would result in excessive wear of the CMG hardware. The filtered command torque is limited and integrated to yield the command momentum. This command momentum is summed with the CMG system momentum to yield the change in CMG system momentum required to correct for the spacecraft errors. The CMG gimbal rates required to provide the desired change in CMG momentum are then calculated by using the steering law. These commands are summed with isogonal corrections and transmitted to the hardware. The response of the hardware is monitored by the CMG gimbal sensors. The gimbal-sensor signals are then used to calculate the control torques generated by the hardware; thereby the simulation loop is closed.

The governing equations for the simulation are presented herein in the order used by the digital computer during each iterative cycle.

SPACECRAFT-TORQUE EQUATIONS

Control-Torque Equations

The control torques applied by the CMG system are computed from the following scalar equations. The CMG gimbal rate and position information required by these equations are supplied by the CMG hardware gimbal sensors. The spacecraft-rate information

is obtained from the previous computer iteration or from the initial conditions since all vehicle sensors are idealized in this simulation. By using the MSFC coordinate system (see appendix), the CMG system control torques are expressed as

$$G_x = H\Big[\left(\dot{\alpha}_1 - \Omega_z\right)\cos\beta_1 \sin\alpha_1 + \left(\dot{\alpha}_3 - \Omega_y\right)\cos\beta_3 \cos\alpha_3 + \left(\Omega_y + \dot{\beta}_1 \cos\alpha_1\right)\sin\beta_1$$

$$- \left(\Omega_z + \dot{\beta}_3 \sin\alpha_3\right)\sin\beta_3 + \left(\Omega_z \cos\alpha_2 + \Omega_y \sin\alpha_2 + \dot{\beta}_2\right)\cos\beta_2\Big] \tag{1a}$$

$$G_y = H\Big[\left(\dot{\alpha}_2 - \Omega_x\right)\cos\beta_2 \sin\alpha_2 + \left(\dot{\alpha}_1 - \Omega_z\right)\cos\beta_1 \cos\alpha_1 + \left(\Omega_z + \dot{\beta}_2 \cos\alpha_2\right)\sin\beta_2$$

$$- \left(\Omega_x + \dot{\beta}_1 \sin\alpha_1\right)\sin\beta_1 + \left(\Omega_x \cos\alpha_3 + \Omega_z \sin\alpha_3 + \dot{\beta}_3\right)\cos\beta_3\Big] \tag{1b}$$

$$G_z = H\Big[\left(\dot{\alpha}_3 - \Omega_y\right)\cos\beta_3 \sin\alpha_3 + \left(\dot{\alpha}_2 - \Omega_x\right)\cos\beta_2 \cos\alpha_2 + \left(\Omega_x + \dot{\beta}_3 \cos\alpha_3\right)\sin\beta_3$$

$$- \left(\Omega_y + \dot{\beta}_2 \sin\alpha_2\right)\sin\beta_2 + \left(\Omega_y \cos\alpha_1 + \Omega_x \sin\alpha_1 + \dot{\beta}_1\right)\cos\beta_1\Big] \tag{1c}$$

These control-torque components are input to both the rigid-body equations and the flexible-body equations for the solution of total-body response.

Disturbance-Torque Equations

The simulation incorporates both the internal- and the external-disturbance torques to which the spacecraft is subjected.

The internal disturbances consist of crew motions in the workshop, in the CSM, and in the LM and are represented in the form of three moments and three forces. The disturbances from crew motions employed in the simulation are either calculated from typical crew-motion profiles, which were obtained by the Space Support Division of the Sperry Rand Corporation under contract to MSFC, programed on the computer or from actual ground-based crew-activity simulation data recorded on magnetic tape for input into the simulation. The equations representing the resultant torque from crew motion are

$$M_{\iota_x} = M_{A_x} + M_{W_x} + M_{J_x} + F_{W_y}L_{W_z} + F_{J_y}L_{J_z} - F_{A_y}L_{A_z} \tag{2a}$$

$$M_{\iota_y} = M_{A_y} + M_{W_y} + M_{J_y} + F_{W_z}L_{W_x} + F_{A_x}L_{A_z} - F_{W_x}L_{W_z}$$

$$- F_{A_z}L_{A_x} - F_{J_x}L_{J_z} - F_{J_z}L_{J_x} \tag{2b}$$

$$M_{\iota_Z} = M_{A_Z} + M_{W_Z} + M_{J_Z} + F_{A_y} L_{A_x} + F_{J_y} L_{J_x} - F_{W_y} L_{W_x} \tag{2c}$$

where the subscripts x, y, and z refer to the body axes and the subscripts A, W, and J refer to the ATM, S-IVB workshop, and CSM areas, respectively. The L_A, L_J, and L_W terms are the moment arms from the crew-motion point of application to the cluster center of gravity and are always taken to be positive. (See fig. 5.) In addition, because of the cluster configuration, the distances along the Y-axis are relatively small; and thus, for the simulation, all crew-motion activity is limited to the X-Z plane.

The forces and moments of equations (1) and (2) also act as disturbances $(GE)_n$ for the flexible body and are defined as

$$\left.\begin{aligned} (GE)_1 &= G_x + M_{A_x} \\ (GE)_2 &= G_y + M_{A_y} \\ (GE)_3 &= G_z + M_{A_z} \\ (GE)_4 &= F_{A_x} \\ (GE)_5 &= F_{A_y} \\ (GE)_6 &= F_{A_z} \end{aligned}\right\} \text{applied at LM location} \tag{3a}$$

$$\left.\begin{aligned} (GE)_7 &= M_{W_x} \\ (GE)_8 &= M_{W_y} \\ (GE)_9 &= M_{W_z} \\ (GE)_{10} &= F_{W_x} \\ (GE)_{11} &= F_{W_y} \\ (GE)_{12} &= F_{W_z} \end{aligned}\right\} \text{applied at S-IVB location} \tag{3b}$$

$$\left.\begin{aligned}(GE)_{13} &= M_{J_x}\\ (GE)_{14} &= M_{J_y}\\ (GE)_{15} &= M_{J_z}\\ (GE)_{16} &= F_{J_x}\\ (GE)_{17} &= F_{J_y}\\ (GE)_{18} &= F_{J_z}\end{aligned}\right\} \text{applied at CSM location} \tag{3c}$$

The external disturbances used in the simulation are limited to the gravity-gradient torques since these torques are the major orbital environment disturbance encountered by the vehicle for its particular mission profile. Therefore, from information obtained by H. F. Kennel at the MSFC, the torques imposed by external disturbances are

$$M_{\epsilon_x} = \frac{3}{2}\Omega_O^2\left(I_{yy} - I_{zz}\right)\left(\sin 2\sigma \cos \xi \sin^2\eta + \cos \sigma \sin \xi \sin 2\eta\right) \tag{4a}$$

$$M_{\epsilon_y} = \frac{3}{2}\Omega_O^2\left(I_{zz} - I_{xx}\right)\left(\sin 2\sigma \sin \xi \sin^2\eta - \cos \sigma \cos \xi \sin 2\eta\right) \tag{4b}$$

$$M_{\epsilon_z} = \frac{3}{2}\Omega_O^2\left(I_{yy} - I_{xx}\right)\left[\sin 2\xi\left(\sin^2\sigma \sin^2\eta - \cos^2\eta\right) - \sin \sigma \cos 2\xi \sin 2\eta\right] \tag{4c}$$

The inertial, orbital, and body-coordinate systems and their relationship used in developing these equations are shown in figure 6.

SPACECRAFT EQUATIONS OF MOTION

Since the ATM cluster is a highly flexible structure, it becomes necessary to define both its rigid and flexible contributions to the total angular motions of the spacecraft.

Rigid-Body Equations

The equations of motion for the rigid-body contribution (assuming negligible products of inertia) to the angular motion of the spacecraft can be expressed as follows:

$$\dot{\Omega}_{R_x} I_{xx} = + \Omega_{R_z} I_{yy} \Omega_{R_y} - \Omega_{R_y} I_{zz} \Omega_{R_z} + T_{R_x} \tag{5a}$$

$$\dot{\Omega}_{R_y} I_{yy} = + \Omega_{R_x} I_{zz} \Omega_{R_z} - \Omega_{R_z} I_{xx} \Omega_{R_x} + T_{R_y} \tag{5b}$$

$$\dot{\Omega}_{R_z} I_{zz} = + \Omega_{R_y} I_{xx} \Omega_{R_x} - \Omega_{R_x} I_{yy} \Omega_{R_y} + T_{R_z} \tag{5c}$$

where the total-torque vector $\{T_R\}$ is defined from equations (1), (2), and (4) as

$$\{T_R\} = \{G\} + \{M_\iota\} + \{M_\epsilon\} \tag{6}$$

These equations are solved for the rigid-body accelerations which are integrated to yield the rigid-body contribution to the vehicle angular rates.

The rigid-body modified Euler angles ϕ_R, θ_R, and ψ_R are derived from the integration of the following differential equations:

$$\begin{Bmatrix} \dot{\phi}_R \\ \dot{\theta}_R \\ \dot{\psi}_R \end{Bmatrix} = \begin{bmatrix} 1 & \tan\theta_R \sin\phi_R & \tan\theta_R \cos\phi_R \\ 0 & \cos\phi_R & -\sin\phi_R \\ 0 & \sec\theta_R \sin\phi_R & \sec\theta_R \cos\phi_R \end{bmatrix} \begin{Bmatrix} \Omega_{R_x} \\ \Omega_{R_y} \\ \Omega_{R_z} \end{Bmatrix} \tag{7}$$

Flexible-Body Equations

The ATM vehicle is represented in this simulation by a modal model truncated to seven dominant modes. The contribution of the flexibility to the body-angular-rate and attitude errors is computed from the equations presented in this section. These equations (see ref. 3) represent a model of the flexibility characteristics of the ATM cluster as obtained from the vibration analysis done under contract to MSFC during the system-design phase.

The modal frequencies and normal modes for the vehicle are found by considering the following generalized equations of motion:

$$[I]\{\ddot{x}\} + K\{x\} = \{GE\} \tag{8}$$

This set of equations can be uncoupled by assuming a solution of the form

$$\{x\} = [\Phi]\{N\} \tag{9}$$

where the $[\Phi]$ matrix represents the varying degree of participation of each normal coordinate in the flexible response.

Since the participation matrix is constant, equation (9) may be differentiated twice to yield

$$\{\ddot{x}\} = [\Phi]\{\ddot{N}\} \tag{10}$$

Inserting equations (9) and (10) into equation (8) forms

$$[I][\Phi]\{\ddot{N}\} + [K][\Phi]\{N\} = \{GE\} \tag{11}$$

This equation may be premultiplied by $[\Phi]^T$ to become

$$[\Phi]^T[I][\Phi]\{\ddot{N}\} + [\Phi]^T[K][\Phi]\{N\} = [\Phi]^T\{GE\} \tag{12}$$

with the conditions

$$[\Phi]^T[I][\Phi] = [1] \tag{13}$$

and

$$[\Phi]^T[K][\Phi] = [\omega^2] \tag{14}$$

which the modal-participation matrix $[\Phi]$ must satisfy. Here, $[1]$ is a diagonal unity matrix, and $[\omega^2]$ is a diagonal matrix containing the squares of the modal frequencies. By considering structural damping, which for the ATM cluster is assumed to be 1 percent of critical damping, the set of equations for the normal modes becomes

$$\{\ddot{N}\} + 2(0.01)[\omega]\{\dot{N}\} + [\omega^2]\{N\} = [\Phi]^T\{GE\} \tag{15}$$

where the $[\Phi]^T$ matrix distributes the generalized force terms over the set of modal equations.

The flexible modes which were represented actively are those which fall within the range of the bending filter, as obtained from work done under contract to MSFC, and control-system bandwidths and are as follows:

Mode number	Modal index	Frequency, Hz
1	1	0.149
3	2	.161
5	3	.414
11	4	.540
14	5	.638
23	6	2.173
25	7	2.52

For the chosen representative flexible modes, equation (15) is partitioned to

$$\ddot{N}_j + 0.02\omega_j\dot{N}_j + \omega_j^2 N_j = [U]_j\{GE\} \tag{16}$$

where $j = 1,2,\ldots,7$ is the modal index and $[U]$ is the 7×18 modal-distribution matrix, given in table I, which is a partition of the elements of the $[\Phi]^T$ matrix.

Equation (10) can be expressed as

$$\Omega_{F_k} = \sum_{\substack{j=1,2,\ldots,7 \\ k=x,y,z}} \phi_{k,j} N_j \tag{17}$$

or

$$\{\Omega_F\} = [P]\{\dot{N}\} \tag{18}$$

where the $[P]$ matrix, presented in table II, is a 3×7 matrix comprised only of the columns of the $[\Phi]$ matrix indicated in the summation. The flexible contribution to the body attitude is then

$$\{\delta\} = \int \{\Omega_F\}\,dt \tag{19}$$

Total-Body Response

The total-body rates are given by

$$\{\Omega\} = \{\Omega_R\} + \{\Omega_F\} \tag{20}$$

The flexible-body attitudes, which are assumed to be small with respect to those of the rigid body, are transformed into Eulerian coordinates by using the following approximation in terms of the rigid-body Euler angles:

$$\begin{Bmatrix} \phi_F \\ \theta_F \\ \psi_F \end{Bmatrix} = \begin{bmatrix} 1 & \tan\theta_R \sin\phi_R & \tan\theta_R \cos\phi_R \\ 0 & \cos\phi_R & -\sin\phi_R \\ 0 & \sec\theta_R \sin\phi_R & \sec\theta_R \cos\phi_R \end{bmatrix} \begin{Bmatrix} \delta_x \\ \delta_y \\ \delta_z \end{Bmatrix} \tag{21}$$

Finally the total-body modified Euler angles representative of spacecraft attitude are given by

$$\begin{Bmatrix} \phi \\ \theta \\ \psi \end{Bmatrix} = \begin{Bmatrix} \phi_R \\ \theta_R \\ \psi_R \end{Bmatrix} + \begin{Bmatrix} \phi_F \\ \theta_F \\ \psi_F \end{Bmatrix} \tag{22}$$

CONTROL-SYSTEM EQUATIONS

Momentum-Feedback Law

The Euler angles and body angular rates developed in the equations of motion are used as the spacecraft signals in the outer-loop control law. The required torque M_c for spacecraft control is expressed as

$$\{M_c\} = \begin{Bmatrix} M_{c_x} \\ M_{c_y} \\ M_{c_z} \end{Bmatrix} = \begin{Bmatrix} K_\phi(\phi - \phi_c) + K_{\dot\phi}(\Omega_x - \Omega_{c_x}) \\ K_\theta(\theta - \theta_c) + K_{\dot\theta}(\Omega_y - \Omega_{c_y}) \\ K_\psi(\psi - \psi_c) + K_{\dot\psi}(\Omega_z - \Omega_{c_z}) \end{Bmatrix} \tag{23}$$

The commanded torque is filtered by fourth-order filters which prevent the high-frequency content caused by the spacecraft flexibility from being included in the CMG system gimbal-rate commands. This filtering of the command torque is required by the bandwidth limitations of the CMG system. The filter transfer functions used in the simulation are the baseline flight-system filters and are given by

$$M_{f_x} = \frac{M_{c_x}}{\left[1 + \frac{2\rho_{f_x} s}{\omega_{f_x}} + \left(\frac{s}{\omega_{f_x}}\right)^2\right]^2} \tag{24a}$$

$$M_{f_y} = \frac{M_{c_y}}{\left[1 + \frac{2\rho_{f_y} s}{\omega_{f_y}} + \left(\frac{s}{\omega_{f_y}}\right)^2\right]^2} \tag{24b}$$

$$M_{f_z} = \frac{M_{c_z}}{\left[1 + \frac{2\rho_{f_z} s}{\omega_{f_z}} + \left(\frac{s}{\omega_{f_z}}\right)^2\right]^2} \tag{24c}$$

These resulting filtered moments are limited to ±200 lbf-ft (271.2 N-m) per axis and then integrated to yield the commanded momentum as shown in figure 7. The command momenta H_c constitute the inputs to the inner loop. It should be noted that H_c has a limit of ±6000 lbf-ft-sec (8136 N-m-sec).

In the control-system inner loop, as shown in figure 4, the CMG momentum vector is calculated from the relationship

$$\{H\} = H \begin{Bmatrix} (\cos \beta_1 \cos \alpha_1) & -(\cos \beta_3 \sin \alpha_3) & -(\sin \beta_2) \\ (\cos \beta_2 \cos \alpha_2) & -(\cos \beta_1 \sin \alpha_1) & -(\sin \beta_3) \\ (\cos \beta_3 \cos \alpha_3) & -(\cos \beta_2 \sin \alpha_2) & -(\sin \beta_1) \end{Bmatrix} \tag{25}$$

The required change in momentum desired from the CMG system to achieve spacecraft control is then

$$\{H_e\} = \{H_c\} - \{H\} \tag{26}$$

The CMG gimbal rates to produce the required momentum change are computed by the steering law of reference 2. The steering-law transformation results in the following commanded CMG gimbal rates:

$$\dot{\beta}_{c_1} = K_{SL_\beta}\left(-H_{e_x} \cos \alpha_1 \sin \beta_1 + H_{e_y} \sin \alpha_1 \sin \beta_1 - H_{e_z} \cos \beta_1\right) \tag{27a}$$

$$\dot{\beta}_{c_2} = K_{SL_\beta}\left(-H_{e_x} \cos \beta_2 - H_{e_y} \cos \alpha_2 \sin \beta_2 + H_{e_z} \sin \alpha_2 \sin \beta_2\right) \tag{27b}$$

$$\dot{\beta}_{c_3} = K_{SL_\beta}\left(H_{e_x} \sin \alpha_3 \sin \beta_3 - H_{e_y} \cos \beta_3 - H_{e_z} \cos \alpha_3 \sin \beta_3\right) \tag{27c}$$

$$\dot{\alpha}_{c_1} = K_{SL_\alpha}\left(-H_{e_x} \sin \alpha_1 - H_{e_y} \cos \alpha_1\right) \tag{27d}$$

$$\dot{\alpha}_{c_2} = K_{SL_\alpha}\left(-H_{e_y} \sin \alpha_2 - H_{e_z} \cos \alpha_2\right) \tag{27e}$$

$$\dot{\alpha}_{c_3} = K_{SL_\alpha}\left(-H_{e_x} \cos \alpha_3 - H_{e_z} \sin \alpha_3\right) \tag{27f}$$

where K_{SL_α} and K_{SL_β} are constants with units of rad/lbf-ft-sec^2 (rad/N-m-sec^2), and H_e is limited to ±33.33 lbf-ft-sec (45.2 N-m-sec) per axis, as in the flight-system design.

Isogonal-Correction Law

Additional gimbal-rate commands to avoid antiparallel conditions are generated by the isogonal correction logic obtained from H. F. Kennel of MSFC. The isogonal computations are performed onboard the spacecraft by a digital computer and, as in the simulation, are updated every 0.25 second.

The isogonal correction consists of two parts: a distribution law which equally distributes the individual CMG momentum vectors about the instantaneous total-system momentum vector and a rotation law which minimizes the CMG inner-gimbal angles.

The input to the digital computer consists of the direction cosines of the momentum components of each individual CMG about each spacecraft axis as follows:

$$E_{1_x} = \cos \beta_1 \cos \alpha_1 \tag{28a}$$

$$E_{1_y} = -\cos \beta_1 \sin \alpha_1 \tag{28b}$$

$$E_{1_z} = -\sin \beta_1 \tag{28c}$$

$$E_{2_x} = -\sin \beta_2 \tag{28d}$$

$$E_{2_y} = \cos \beta_2 \cos \alpha_2 \tag{28e}$$

$$E_{2_z} = -\cos \beta_2 \sin \alpha_2 \tag{28f}$$

$$E_{3_x} = -\cos \beta_3 \sin \alpha_3 \tag{28g}$$

$$E_{3_y} = -\sin \beta_3 \tag{28h}$$

$$E_{3_z} = \cos \beta_3 \cos \alpha_3 \tag{28i}$$

The distribution- and rotation-law gains used by the isogonal computer are K_{DP} and K_r, respectively. Additional direction cosines not available from the hardware are computed as follows:

$$\left.\begin{aligned} E'_{1_z} &= \sqrt{\left(1 - E^2_{1_z}\right)^{-1}} \\ E'_{2_x} &= \sqrt{\left(1 - E^2_{2_x}\right)^{-1}} \\ E'_{3_y} &= \sqrt{\left(1 - E^2_{3_y}\right)^{-1}} \end{aligned}\right\} \tag{29}$$

The total CMG system momentum E_T and the total components about each spacecraft axis are

$$\left.\begin{aligned} E_{T_x} &= E_{1_x} + E_{2_x} + E_{3_x} \\ E_{T_y} &= E_{1_y} + E_{2_y} + E_{3_y} \\ E_{T_z} &= E_{1_z} + E_{2_z} + E_{3_z} \\ E^2_T &= E^2_{T_x} + E^2_{T_y} + E^2_{T_z} \\ E_T &= \sqrt{E^2_T} \end{aligned}\right\} \tag{30}$$

and the solution of the determinant of direction cosines for the angular-momentum vectors becomes

$$q = E_{1_X}\left(E_{2_y}E_{3_Z} - E_{3_y}E_{2_Z}\right) + E_{2_X}\left(E_{3_y}E_{1_Z} - E_{1_y}E_{3_Z}\right) + E_{3_X}\left(E_{1_y}E_{2_Z} - E_{2_y}E_{1_Z}\right)$$

$$\begin{pmatrix} \text{sgn } q = +1 \quad \text{for} \quad q \geqq 0 \\ \text{sgn } q = -1 \quad \text{for} \quad q < 0 \end{pmatrix} \tag{31}$$

where $q \geqq 0$ defines a right-handed system and $q < 0$ defines a left-handed system of direction-cosine vectors. This information is used to determine the sign of the distribution-law gain. The magnitude of the distribution-law gain λ is variable and is determined from the magnitude of the total-system momentum vector E_T with maximum gain occurring in the region of antiparallelism $\left(E_T \approx 1\right)$

$$\left.\begin{array}{lll} \lambda = 0 & \text{for} & E_T \leqq 0.25 \\ \lambda = 2E_T - 0.5 & \text{for} & 0.25 < E_T \leqq 0.75 \\ \lambda = +1 & \text{for} & 0.75 < E_T \leqq 1.25 \\ \lambda = +3.5 - 2E_T & \text{for} & 1.25 < E_T \leqq 1.65 \\ \lambda = +0.2 & \text{for} & 1.65 < E_T \end{array}\right\} \tag{32}$$

The actual distribution-law gain expressed as a function of λ thus becomes

$$K_D = K_{DP}\left[(\text{sgn } q)\lambda\right] \tag{33}$$

The following computations yield the CMG gimbal rates required to maintain the isogonal distribution and to minimize the CMG inner-gimbal angles. The distribution-law calculation involves taking the dot product of each individual CMG momentum vector and the total-system momentum vector and commanding gimbal rates which will equalize these dot products while maintaining constant system momentum. The rotation law commands CMG precession rates to minimize mean inner-gimbal angles. These required precession rates are then transformed into CMG gimbal coordinates to yield gimbal-rate commands as follows:

$$\left.\begin{aligned} (BE)_X &= E_{2_X}E_{3_X} + E_{2_y}E_{3_y} + E_{2_Z}E_{3_Z} \\ (BE)_y &= E_{1_X}E_{3_X} + E_{1_y}E_{3_y} + E_{1_Z}E_{3_Z} \\ (BE)_Z &= E_{1_X}E_{2_X} + E_{1_y}E_{2_y} + E_{1_Z}E_{2_Z} \end{aligned}\right\} \tag{34}$$

$$\left.\begin{aligned} e_{I_x} &= \left[(BE)_z - (BE)_y\right]K_D \\ e_{I_y} &= \left[(BE)_x - (BE)_z\right]K_D \\ e_{I_z} &= \left[(BE)_y - (BE)_x\right]K_D \end{aligned}\right\} \tag{35}$$

$$\left.\begin{aligned} H_{1_x} &= e_{I_z}E_{2_x} + e_{I_y}E_{3_x} \\ H_{1_y} &= e_{I_z}E_{2_y} + e_{I_y}E_{3_y} \\ H_{1_z} &= e_{I_z}E_{2_z} + e_{I_y}E_{3_z} \\ H_{2_x} &= e_{I_x}E_{3_x} + e_{I_z}E_{1_x} \\ H_{2_y} &= e_{I_x}E_{3_y} + e_{I_z}E_{1_y} \\ H_{2_z} &= e_{I_x}E_{3_z} + e_{I_z}E_{1_z} \\ H_{3_x} &= e_{I_y}E_{1_x} + e_{I_x}E_{2_x} \\ H_{3_y} &= e_{I_y}E_{1_y} + e_{I_x}E_{2_y} \\ H_{3_z} &= e_{I_y}E_{1_z} + e_{I_x}E_{2_z} \end{aligned}\right\} \tag{36}$$

$$\left.\begin{aligned} e_{r_1} &= \frac{E_{1_z}\left(E'_{1_z}\right)^2\left(E_{1_y}E_{T_x} - E_{1_x}E_{T_y}\right)}{K_r} \\ e_{r_2} &= \frac{E_{2_x}\left(E'_{2_x}\right)^2\left(E_{2_z}E_{T_y} - E_{2_y}E_{T_z}\right)}{K_r} \\ e_{r_3} &= \frac{E_{3_y}\left(E'_{3_y}\right)^2\left(E_{3_x}E_{T_z} - E_{3_z}E_{T_x}\right)}{K_r} \\ e_r &= \frac{K_r}{E_T^2}\left(e_{r_1} + e_{r_2} + e_{r_3}\right) \end{aligned}\right\} \tag{37}$$

$$
\left.
\begin{aligned}
R_{1_x} &= H_{1_x} + e_r E_{T_x} \\
R_{1_y} &= H_{1_y} + e_r E_{T_y} \\
R_{1_z} &= H_{1_z} + e_r E_{T_z} \\
R_{2_x} &= H_{2_x} + e_r E_{T_x} \\
R_{2_y} &= H_{2_y} + e_r E_{T_y} \\
R_{2_z} &= H_{2_z} + e_r E_{T_z} \\
R_{3_x} &= H_{3_x} + e_r E_{T_x} \\
R_{3_y} &= H_{3_y} + e_r E_{T_y} \\
R_{3_z} &= H_{3_z} + e_r E_{T_z}
\end{aligned}
\right\} \tag{38}
$$

The CMG gimbal rates commanded by the isogonal computer are

$$
\left.
\begin{aligned}
\dot{\beta}_{CI_1} &= -E'_{1_z}\left(E_{1_y}R_{1_x} - E_{1_x}R_{1_y}\right) \\
\dot{\alpha}_{CI_1} &= \left(E'_{1_z}\right)^2 E_{1_z}\left(E_{1_x}R_{1_x} + E_{1_y}R_{1_y}\right) - R_{1_z} \\
\dot{\beta}_{CI_2} &= -E'_{2_x}\left(E_{2_z}R_{2_y} - E_{2_y}R_{2_z}\right) \\
\dot{\alpha}_{CI_2} &= \left(E'_{2_x}\right)^2 E_{2_x}\left(E_{2_y}R_{2_y} + E_{2_z}R_{2_z}\right) - R_{2_x} \\
\dot{\beta}_{CI_3} &= -E'_{3_y}\left(E_{3_x}R_{3_z} - E_{3_z}R_{3_x}\right) \\
\dot{\alpha}_{CI_3} &= \left(E'_{3_y}\right)^2 E_{3_y}\left(E_{3_z}R_{3_z} + E_{3_x}R_{3_x}\right) - R_{3_y}
\end{aligned}
\right\} \tag{39}
$$

The isogonal-correction commands are limited to $\pm 1^{\circ}$/sec as in the flight system.

The steering-law commands (eqs. (27)) are summed with the isogonal-correction commands (eqs. (39)) to yield total CMG gimbal-rate commands which are then fed to the hardware. The total CMG gimbal-rate commands are limited to a maximum of $\pm 3.5^{\circ}$/sec to avoid overstressing the CMG rotor of the flight hardware.

CMG HARDWARE DESCRIPTION

The hardware utilized in the real-time digital-hardware simulation of the ATM flight consists of three full-scale CMG's with a momentum capacity of 1000 lbf-ft-sec (1356 N-m-sec) per gyroscope. The CMG's are statically mounted on a unitized rigid test stand. (See fig. 8.) Each CMG is a double-gimbaled device which produces torque by precession of a constant-speed inertia wheel. Each gimbal is provided with a direct-current torquer acting through a compound planetary gear train and with gimbal-rate and position monitors. Excitation to the spin motors and gimbal torquers is provided through the electronics located in the master-control room. (See fig. 9.) Link between the CMG hardware and the digital computer is effected through the signal-buffer system in the master-control room.

The CMG gimbals are driven and controlled by a rate servo loop (fig. 10) which uses a tachometer to monitor gimbal-torquer speed rather than actual gimbal rate as the feedback element. This servo-loop design was predicated on the need for a high-gain servo loop to provide adequate transient response and on the assumption that the gear train provided a stiff link between the torquer and the gimbal.

From figure 11, it can be seen that the servo loop using the motor tachometer results in a bandwidth of approximately 150 rad/sec at the 90^{o} phase point. This bandwidth would appear to be more than adequate to meet all the control requirements for manned vehicles such as the ATM. However, in monitoring the actual gimbal rate by means of a tachometer located after the gear train, large bandwidth discrepancies were noted. As can be observed from figure 12, the servo-loop bandwidth based on actual gimbal rate is only about 20 rad/sec at the 90^{o} phase point. The drastic reduction in frequency response was thought to be caused by excessive cross coupling between gimbals or by the fact that a rigid link between motor and gimbal did not exist as originally was assumed. Therefore, tests were made with one gimbal mechanically locked, thereby virtually eliminating the gimbal cross-coupling effects. The servo-loop bandwidth was not appreciably affected (fig. 13); and cross coupling was thus eliminated as the major cause for the loss in frequency response. Furthermore, the gimbal-tachometer output was monitored to observe gimbal response to sinusoidal and step inputs. For sinusoidal inputs, it was noted that a frequency was reached at which no torque or resultant motion was transmitted through the gear train to the gimbal. It should be recalled that the amplitude of the excursion or travel of a system such as a gear train will decrease as the frequency of the sinusoidal input is increased since less time elapses between command reversals. Thus, for commanded frequencies at which the excursion amplitude is equal to or less than the gear-train dead band, no gimbal motion will occur. The frequency

response of the CMG is therefore directly limited by this gear-train effect. Windup effects of the gear train caused by low stiffness introduce a time lag between input and output as well as overshoots in the output. Other servo loops have been tested on the hardware with no gain in bandwidth or time constant again because of gear-train limitations. Gear-train improvement is therefore necessary for better CMG hardware response.

SIMULATION PROBLEMS

The real-time simulation is conducted with the aid of a Control Data 6600 digital computer. However, the CMG hardware used in this simulation is an analog device. Thus, conversion equipment to transmit signals between the digital and analog realms is required. The 14-bit plus sign-conversion equipment utilized in this simulation has a resolution of approximately 1 part in 16 000 (2^{14}). However, because of the momentum-feedback control-law requirement for high resolution in the gimbal-position signals, this equipment was found to be inadequate, even though it is the best commercially available equipment. This lack in resolution was demonstrated by a flicker in the last bit of the analog-digital converter through which the CMG gimbal angles are passed. This flicker had an equivalent amplitude of 0.6 millivolt; and because of the simulation gains (fig. 3), the flicker resulted in a rate-command error of one-fifth of the full-scale command. An attempt at eliminating the problem by programing the simulation inner loop on an analog computer proved unsuccessful since the simulation gain remained unchanged and the analog-digital converters were still required. The solution to this problem was found in the use of a compensation-filter scheme employed to compensate for the detrimental gear-train effects and is discussed in the following section.

SYSTEM PROBLEMS

The gear trains furnished with the CMG hardware exhibited an output stiffness of 47 000 lbf-ft/rad (63.7 kN-m/rad) and a backlash of over 6^{o} at the input (0.1^{o} at the output). This excessive dead band resulted in an unstable system at the system-design gains. As is evident from figure 14, a stable system was obtained for a maximum inner-loop gain (K_{SL}) of 0.000875 rad/lbf-ft-sec^2 (0.000645 rad/N-m-sec^2), which is about one order of magnitude lower than the ATM flight-design gain. (See ref. 2.)

To meet the ATM mission pointing requirements, it became necessary to try to improve the CMG hardware. The corrective measures to improve CMG performance involved decreasing the gear-train backlash by plating the gears and increasing the gear-pivot-bearing preloads. A plot of average gimbal-rate limit cycling (with no spacecraft disturbances) for increasing inner-loop gain (fig. 15) illustrates the improvement. The

gear-train backlash is evidently still much too large for the system to perform all of the required control tasks. Thus, the resulting system performance was still unacceptable since the inner-loop gain was still below the design value and because limit-cycle amplitudes were still too large. (See fig. 16.) A compensation-filtering scheme by Willard W. Anderson of the Langley Research Center for the position signals was incorporated in the simulation. (See fig. 4.) This scheme maintains the actual gimbal position in the low-frequency region but alters the actual position on a high-frequency basis in calculating the system momentum. This alteration is accomplished by adding the commanded gimbal rate to the position signal and then filtering the sum. The position signal used by the computer is thus

$$\alpha = \frac{\alpha_{gimbal} + K_a\dot{\alpha}_{command}}{1 + K_a s} \tag{40}$$

This compensation filter eliminates the high-frequency limit cycle induced by the phase lag associated with the actual gimbal position due to gear-train backlash. Thus, for the low-frequency region

$$\frac{\alpha_{gimbal} + K_a\dot{\alpha}_{command}}{1 + K_a s} \approx \alpha_{gimbal}$$

and for the high-frequency region

$$\frac{\alpha_{gimbal} + K_a\dot{\alpha}_{command}}{1 + K_a s} \approx \alpha_{command}$$

This scheme also allows for continuous updating of the gimbal position. Figures 16, 17(a), and 17(b) present limit-cycle amplitudes for full inner-loop-design gains $\left(K_{SL} = 0.00525 \text{ rad/lbf-ft-sec}^2 \ (0.00387 \text{ rad/N-m-sec}^2)\right)$ for compensation gains K_a of 0, 1.0, and 6.0 seconds. For values of $K_a > 6.0$ seconds, the inner-loop-limit cycle is no longer noticeable. The benefits of the compensation-filter scheme are further evidenced by the data presented in figure 18. The compensation-filter gain was set at $K_a = 16.0$ seconds and the system subjected to a three-axis maneuver of 0.05^o. As can be seen, no noticeable inner-loop-limit cycle is present after completion of the maneuver. The apparent gimbal rate observed at the end of the maneuver in the data of figures 17 and 18 is a result of recorder zero offset and not a product of the simulation.

The difficulties encountered with the gear-train backlash in this simulation is a serious system problem primarily caused by the momentum-feedback-loop sensitivity to the small variations in CMG characteristics.

Subsequent simulations will include the control-moment gyroscopes mounted in torque-measurement fixtures to provide direct-control torque input to the computer. This combination will be mounted in a dynamic environment provided by a three-axis servo table (fig. 19) utilized to represent the spacecraft motions. Simulations to determine manual control feasibility will also be conducted by including a pilot control console (fig. 20) in the simulation loop.

CONCLUDING REMARKS

A description of a real-time digital-computer-hardware simulation of an Apollo-Telescope-Mount mission has been presented. Problems encountered during the investigation consisted of both simulation and system problems.

The simulation problem was caused by the resolution limitation of the conversion equipment. This limitation introduced an erroneous control-moment-gyroscope (CMG) gimbal-rate command equal to one-fifth of the full-scale gimbal-rate command.

The system problem was an excessive limit cycle of the spacecraft during the fine-pointing mode. This limit cycle was directly attributed to the CMG gimbal actuators. These actuators exhibited high-backlash and low-stiffness characteristics which resulted in an unstable system for the system design gains.

The solution to both of these problems was found in the use of a compensation-filtering scheme for the position-feedback signals from the hardware. This scheme maintains the actual gimbal position in the low-frequency region but alters the actual position on a high-frequency basis in the calculation of the system momentum. The compensation-filtering scheme utilized in this simulation was effective in alleviating the sensitivity of the momentum-feedback control law to small variations in CMG characteristics. The employment of this scheme resulted in a stable system at the system design gains and thus permitted a complete system evaluation.

Langley Research Center,
National Aeronautics and Space Administration,
Hampton, Va., June 11, 1970.

APPENDIX

COORDINATE SYSTEM

The axis placement and positive gimbal-angle notation for the control-moment gyroscope oriented as suggested by researchers at the Marshall Space Flight Center are defined by the following sketch:

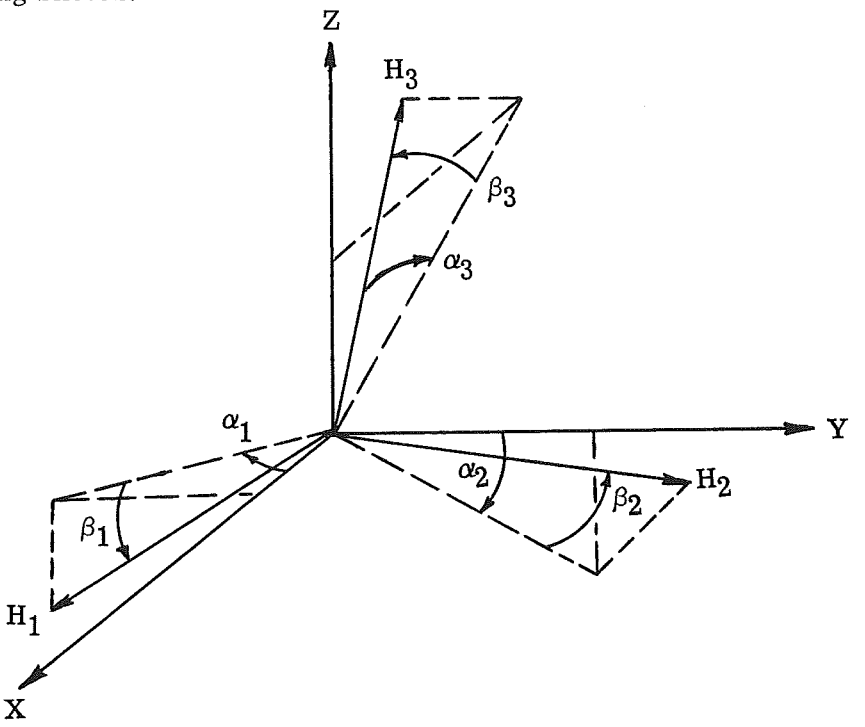

Outer-gimbal angles are denoted with the symbol α and inner-gimbal angles with β. For nominal inner-gimbal angles, $\beta_1 = \beta_2 = \beta_3 = 0^o$, the outer-gimbal rate $\dot{\alpha}_1$ is about the -Z spacecraft axis, $\dot{\alpha}_2$ about the -X spacecraft axis, and $\dot{\alpha}_3$ about the -Y spacecraft axis.

REFERENCES

1. Kurzhals, Peter R.; and Grantham, Carolyn: A System for Inertial Experiment Pointing and Attitude Control. NASA TR R-247, 1966.

2. Chubb, W. B.; Schultz, D. W.; and Seltzer, S. M.: Attitude Control and Precision Pointing of the Apollo Telescope Mount. AIAA Pap. No. 67-534, Aug. 1967.

3. Halfman, Robert L.: Dynamics. Vol. II – Systems, Variational Methods, and Relativity. Addison-Wesley Pub. Co., Inc., c.1962.

TABLE I.- MODAL-DISTRIBUTION MATRIX

$$[U]^T = \begin{bmatrix}
4.40 \times 10^{-4} & -4.27 \times 10^{-4} & 6.91 \times 10^{-3} & -2.21 \times 10^{-3} & -1.21 \times 10^{-4} & 2.21 \times 10^{-3} & -2.92 \times 10^{-3} \\
4.80 \times 10^{-6} & -8.40 \times 10^{-6} & -7.44 \times 10^{-5} & 1.50 \times 10^{-4} & -8.44 \times 10^{-3} & -8.88 \times 10^{-5} & -6.60 \times 10^{-5} \\
2.28 \times 10^{-5} & -2.28 \times 10^{-5} & 2.41 \times 10^{-4} & -6.72 \times 10^{-5} & -3.60 \times 10^{-6} & -1.89 \times 10^{-3} & -1.01 \times 10^{-2} \\
3.00 \times 10^{-5} & -6.00 \times 10^{-5} & -4.60 \times 10^{-4} & 6.90 \times 10^{-4} & -2.99 \times 10^{-2} & 7.00 \times 10^{-5} & 2.80 \times 10^{-4} \\
4.22 \times 10^{-3} & -4.41 \times 10^{-3} & 1.73 \times 10^{-3} & 4.64 \times 10^{-3} & 5.20 \times 10^{-4} & -2.15 \times 10^{-2} & 3.65 \times 10^{-2} \\
-9.00 \times 10^{-5} & -8.90 \times 10^{-4} & 7.90 \times 10^{-4} & -5.70 \times 10^{-4} & 6.07 \times 10^{-3} & -4.28 \times 10^{-3} & -1.54 \times 10^{-3} \\
7.28 \times 10^{-4} & -7.92 \times 10^{-4} & -6.20 \times 10^{-3} & 3.38 \times 10^{-3} & 2.44 \times 10^{-4} & 2.57 \times 10^{-4} & -3.52 \times 10^{-4} \\
4.80 \times 10^{-6} & -7.20 \times 10^{-6} & -3.72 \times 10^{-5} & 2.64 \times 10^{-5} & 6.01 \times 10^{-4} & -1.70 \times 10^{-4} & -6.48 \times 10^{-5} \\
2.16 \times 10^{-5} & -2.16 \times 10^{-5} & 1.96 \times 10^{-4} & -5.04 \times 10^{-5} & -4.80 \times 10^{-6} & 1.65 \times 10^{-3} & -1.88 \times 10^{-3} \\
-2.00 \times 10^{-5} & 4.00 \times 10^{-5} & 2.40 \times 10^{-4} & -4.80 \times 10^{-4} & 2.50 \times 10^{-2} & -6.20 \times 10^{-4} & 2.30 \times 10^{-4} \\
-1.55 \times 10^{-3} & 1.57 \times 10^{-3} & -9.62 \times 10^{-3} & 1.90 \times 10^{-3} & -2.00 \times 10^{-5} & -1.21 \times 10^{-2} & 2.25 \times 10^{-2} \\
-2.60 \times 10^{-4} & -6.10 \times 10^{-4} & 2.16 \times 10^{-3} & -1.57 \times 10^{-3} & -1.32 \times 10^{-2} & -1.29 \times 10^{-3} & -3.00 \times 10^{-5} \\
7.28 \times 10^{-4} & -7.90 \times 10^{-4} & -6.11 \times 10^{-3} & 3.37 \times 10^{-3} & 2.45 \times 10^{-4} & 1.13 \times 10^{-4} & -6.96 \times 10^{-5} \\
4.80 \times 10^{-6} & -8.40 \times 10^{-6} & -3.84 \times 10^{-5} & 3.12 \times 10^{-5} & 3.98 \times 10^{-4} & 4.80 \times 10^{-4} & 1.37 \times 10^{-4} \\
2.28 \times 10^{-5} & -2.40 \times 10^{-5} & 2.54 \times 10^{-4} & -7.08 \times 10^{-5} & -7.20 \times 10^{-6} & -3.25 \times 10^{-3} & 5.41 \times 10^{-3} \\
-2.00 \times 10^{-5} & 4.00 \times 10^{-5} & 2.40 \times 10^{-4} & -4.80 \times 10^{-4} & 2.50 \times 10^{-2} & -6.50 \times 10^{-4} & 2.70 \times 10^{-4} \\
-3.08 \times 10^{-3} & 3.11 \times 10^{-3} & -2.47 \times 10^{-2} & 5.98 \times 10^{-3} & 3.90 \times 10^{-4} & 5.47 \times 10^{-2} & -9.20 \times 10^{-2} \\
6.00 \times 10^{-5} & -1.14 \times 10^{-3} & -4.10 \times 10^{-4} & 4.00 \times 10^{-4} & 1.83 \times 10^{-2} & 9.55 \times 10^{-3} & 2.38 \times 10^{-3}
\end{bmatrix}$$

TABLE II.- MODAL-PARTICIPATION MATRIX

$$[P] = \begin{bmatrix} 3.67 \times 10^{-5} & -3.56 \times 10^{-5} & 5.76 \times 10^{-4} & -1.841 \times 10^{-4} & -1.010 \times 10^{-5} & 1.838 \times 10^{-4} & -2.432 \times 10^{-4} \\ 4.00 \times 10^{-7} & -7.00 \times 10^{-7} & -6.20 \times 10^{-6} & 1.250 \times 10^{-5} & -7.031 \times 10^{-4} & -7.400 \times 10^{-6} & -5.500 \times 10^{-6} \\ 1.90 \times 10^{-6} & -1.90 \times 10^{-6} & 2.01 \times 10^{-5} & -5.600 \times 10^{-6} & -3.000 \times 10^{-7} & -1.573 \times 10^{-4} & -8.388 \times 10^{-4} \end{bmatrix}$$

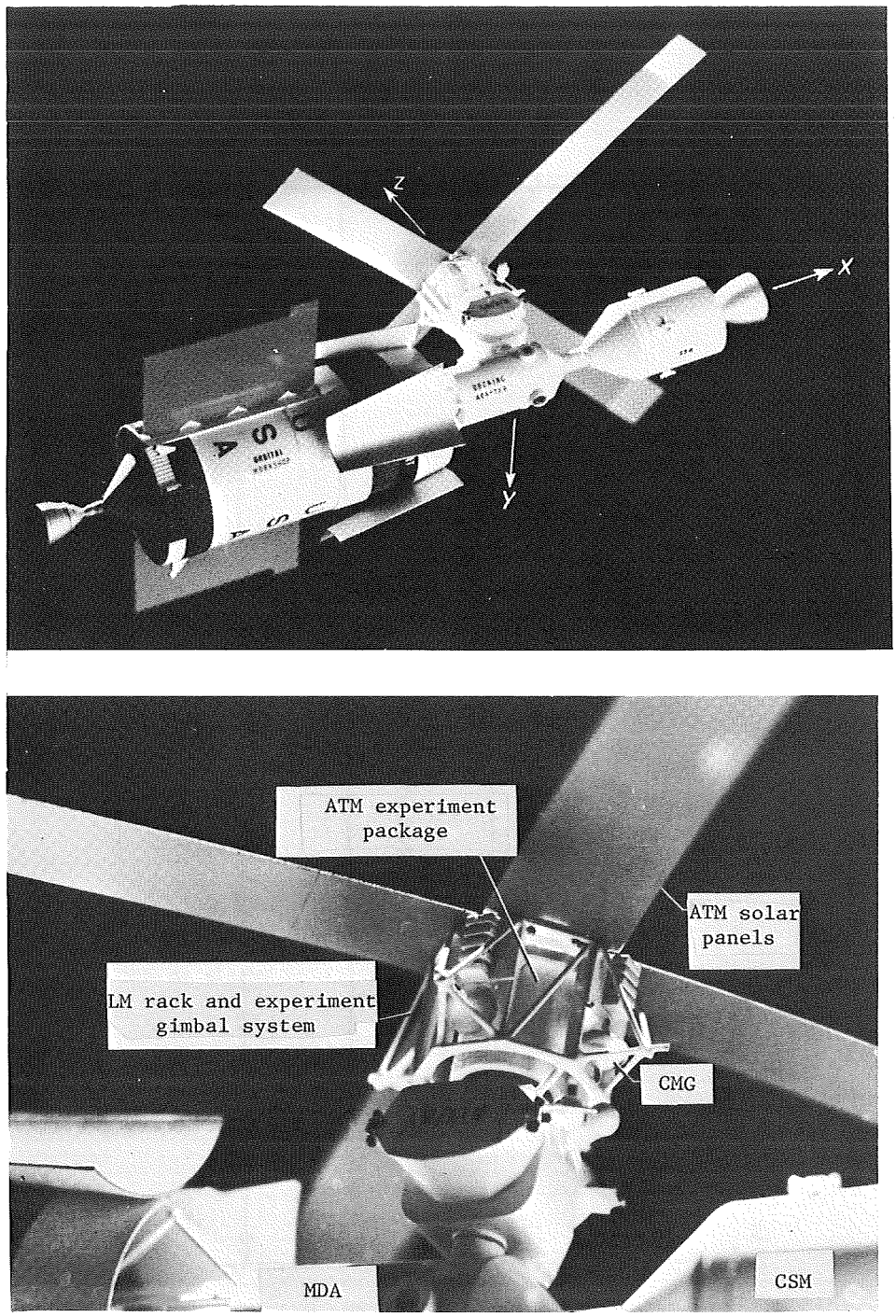

Figure 1.- Photographs of ATM cluster. L-70-1659

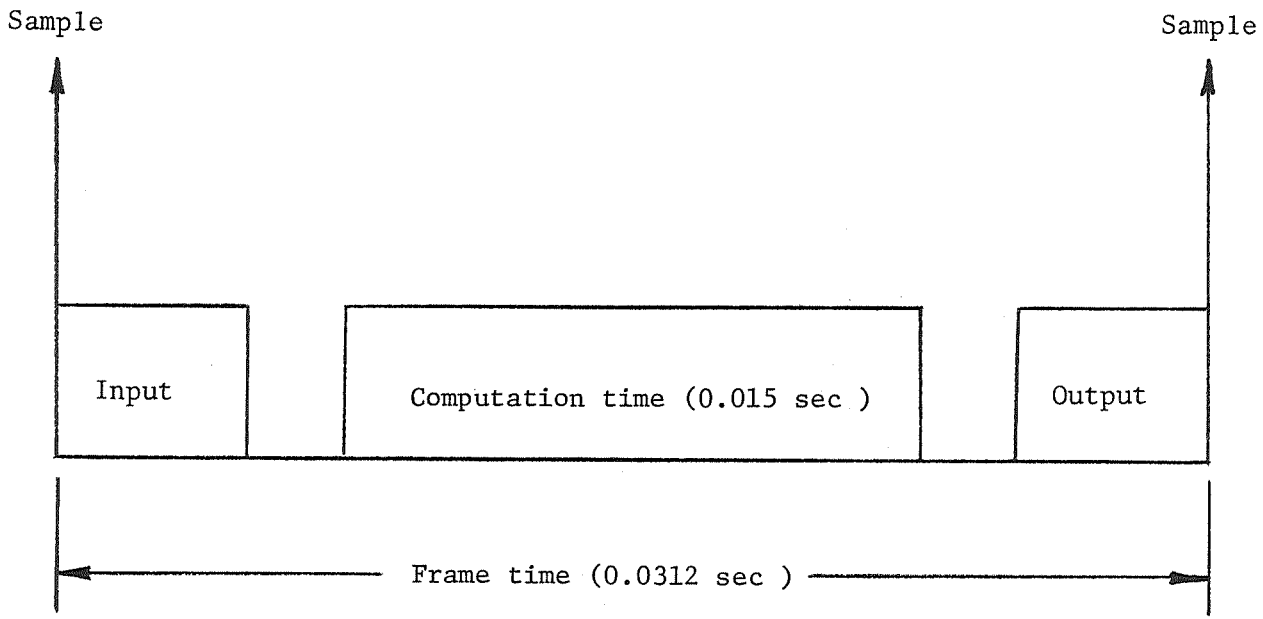

Figure 2.- Simulation iteration cycle.

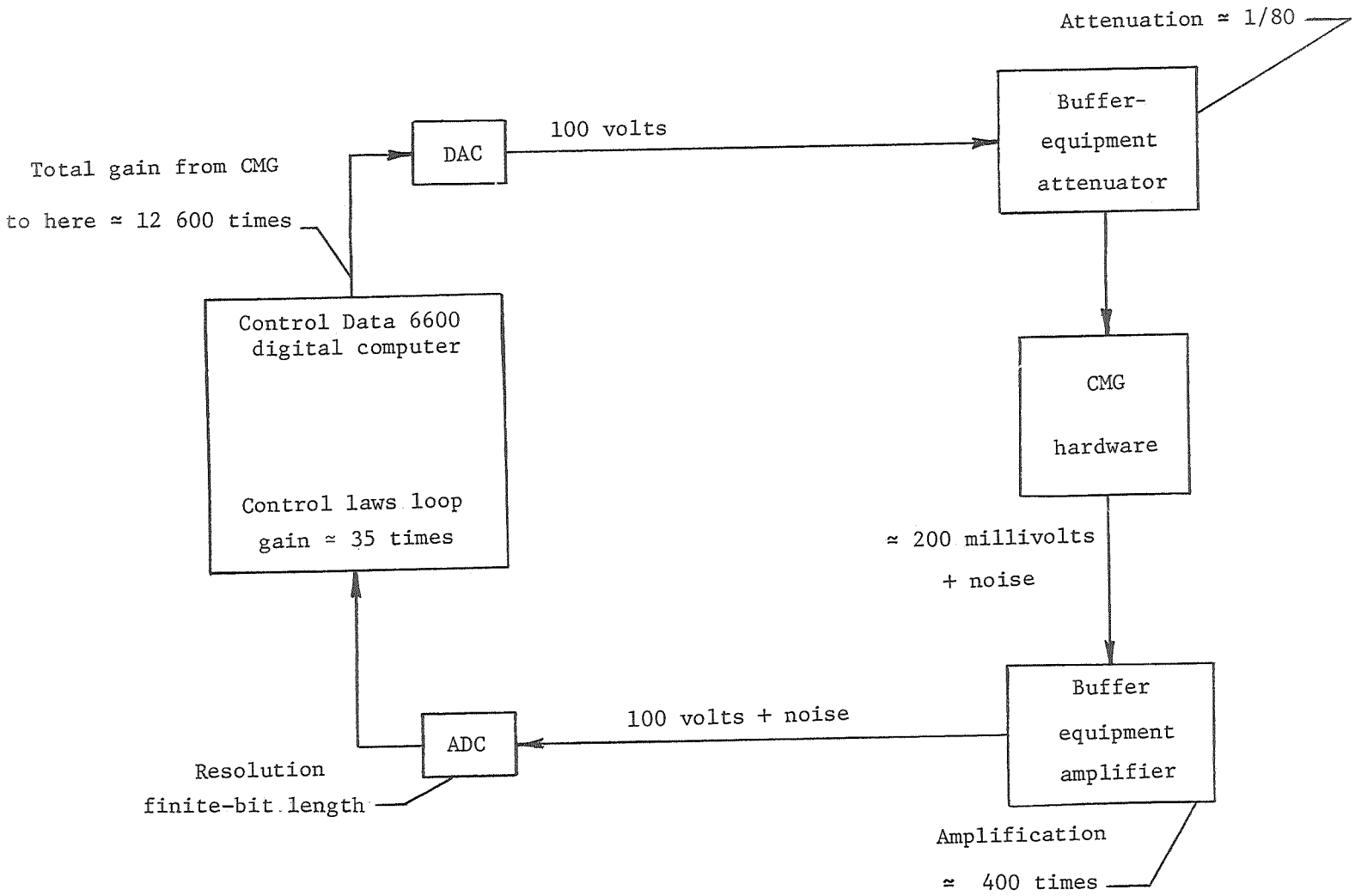

Figure 3.- Simulation concept and scaling.

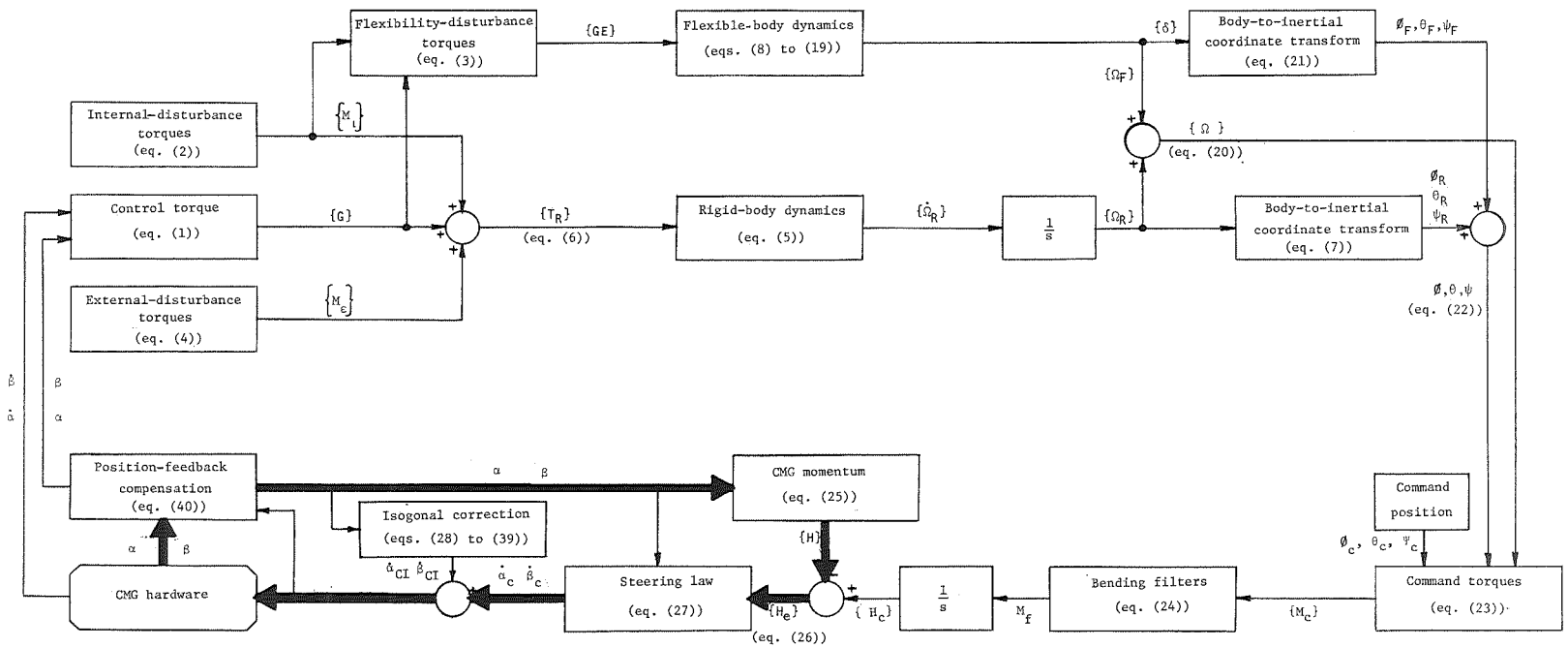

Figure 4.- Block diagram of simulation.

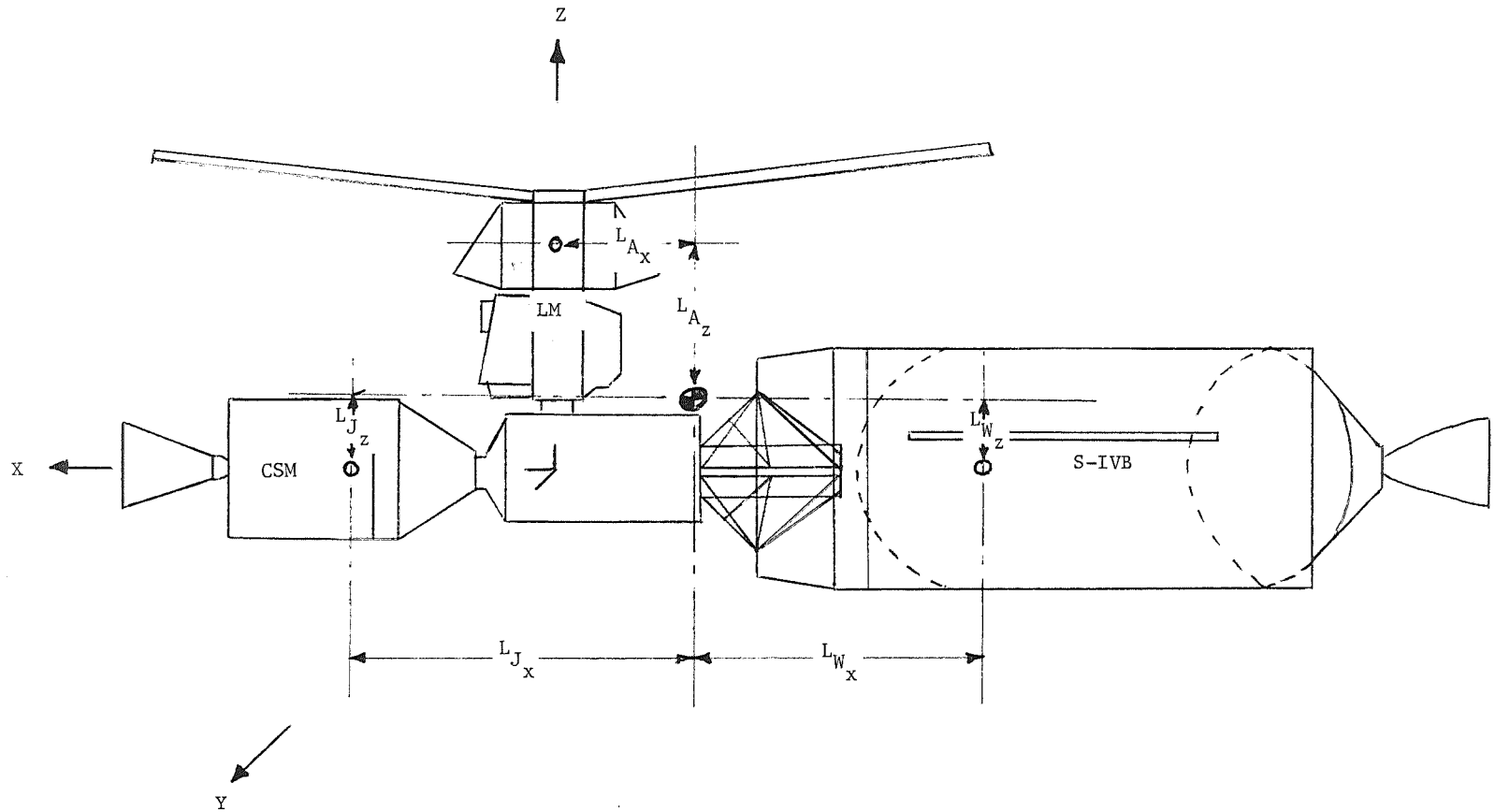

Figure 5.- Location of crew-motion activity.

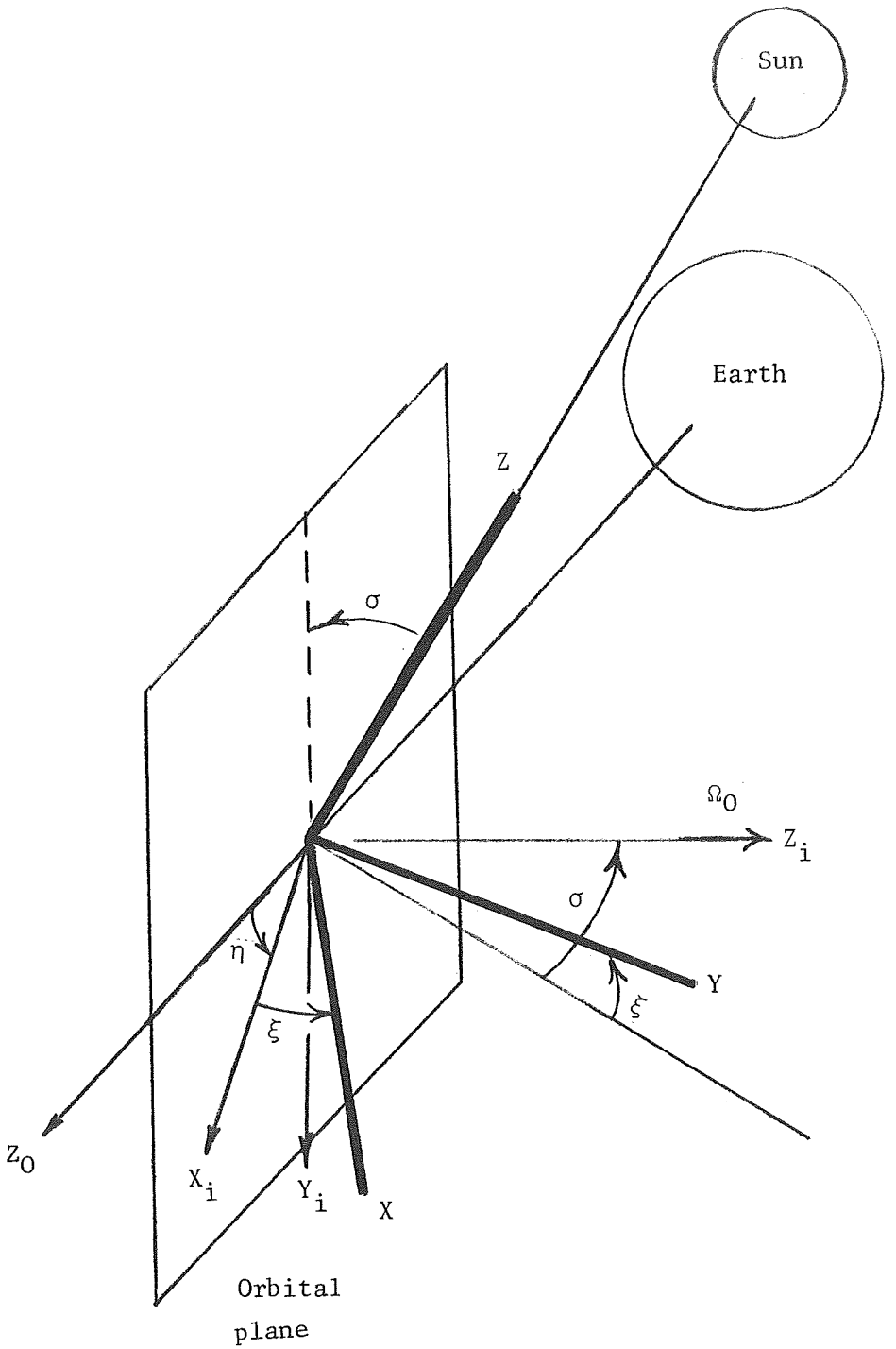

Figure 6.- Coordinate system for external-disturbance torques.

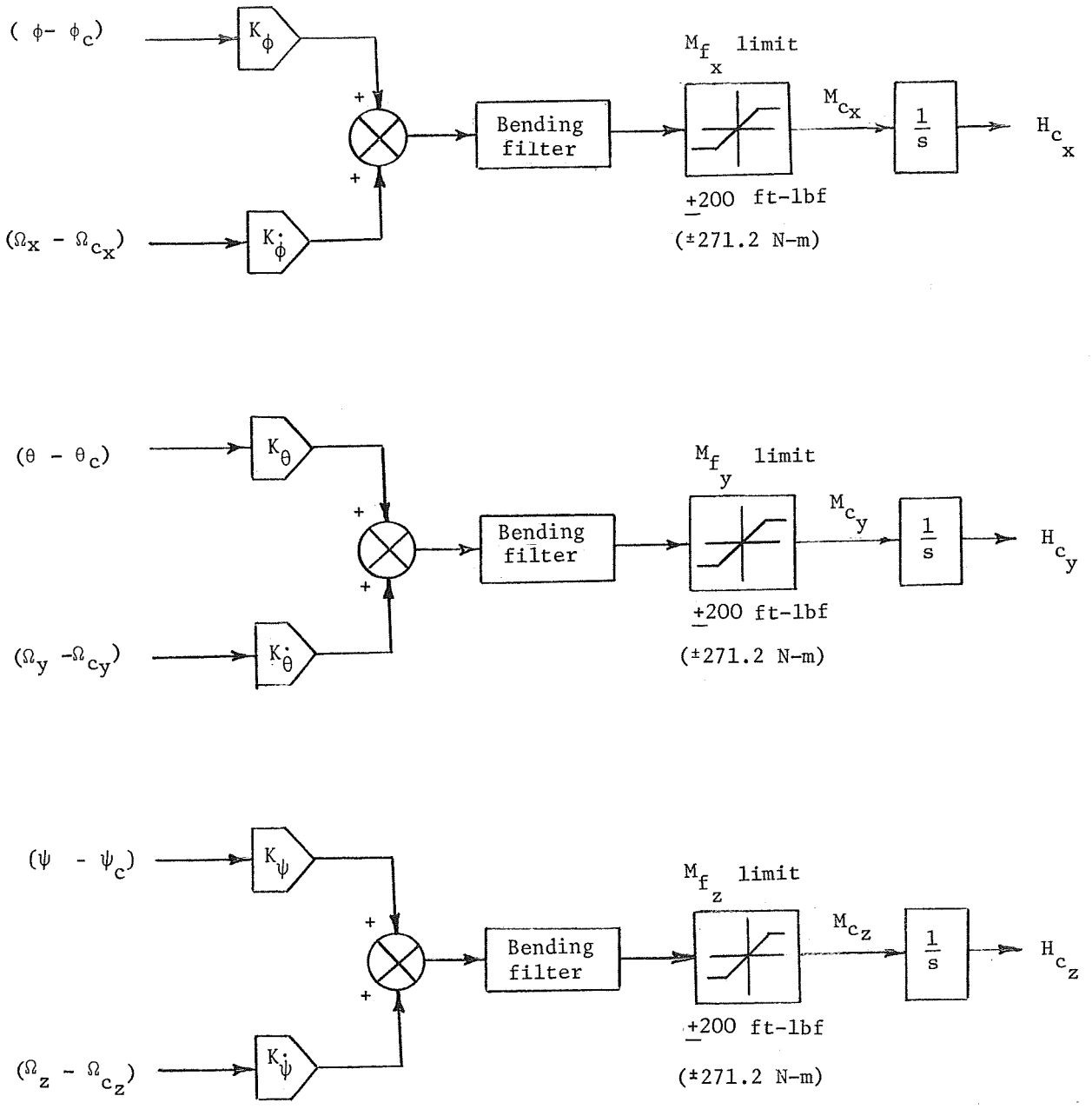

Figure 7.- Schematic drawing of command law.

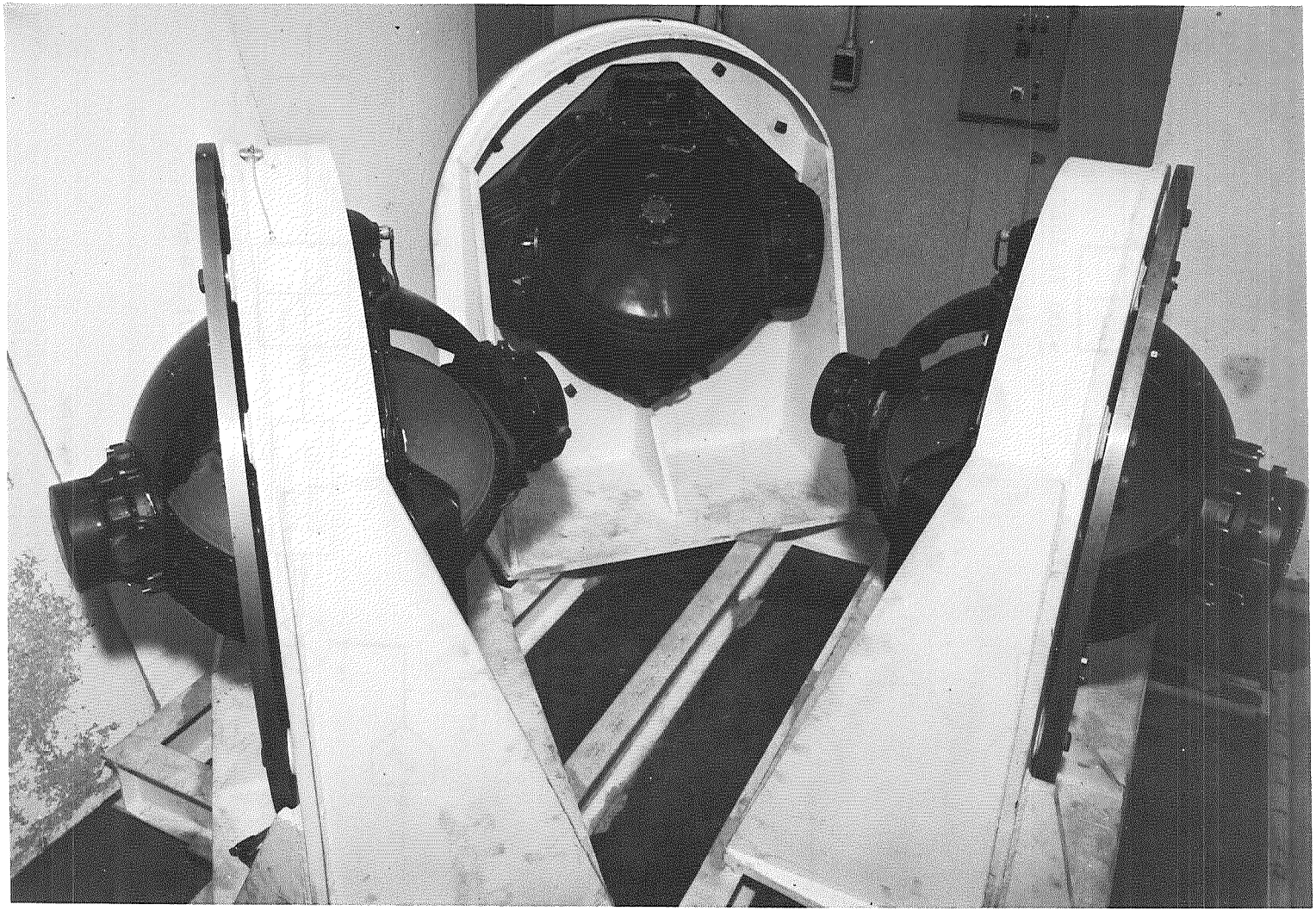

Figure 8.- CMG static test setup. L-68-686

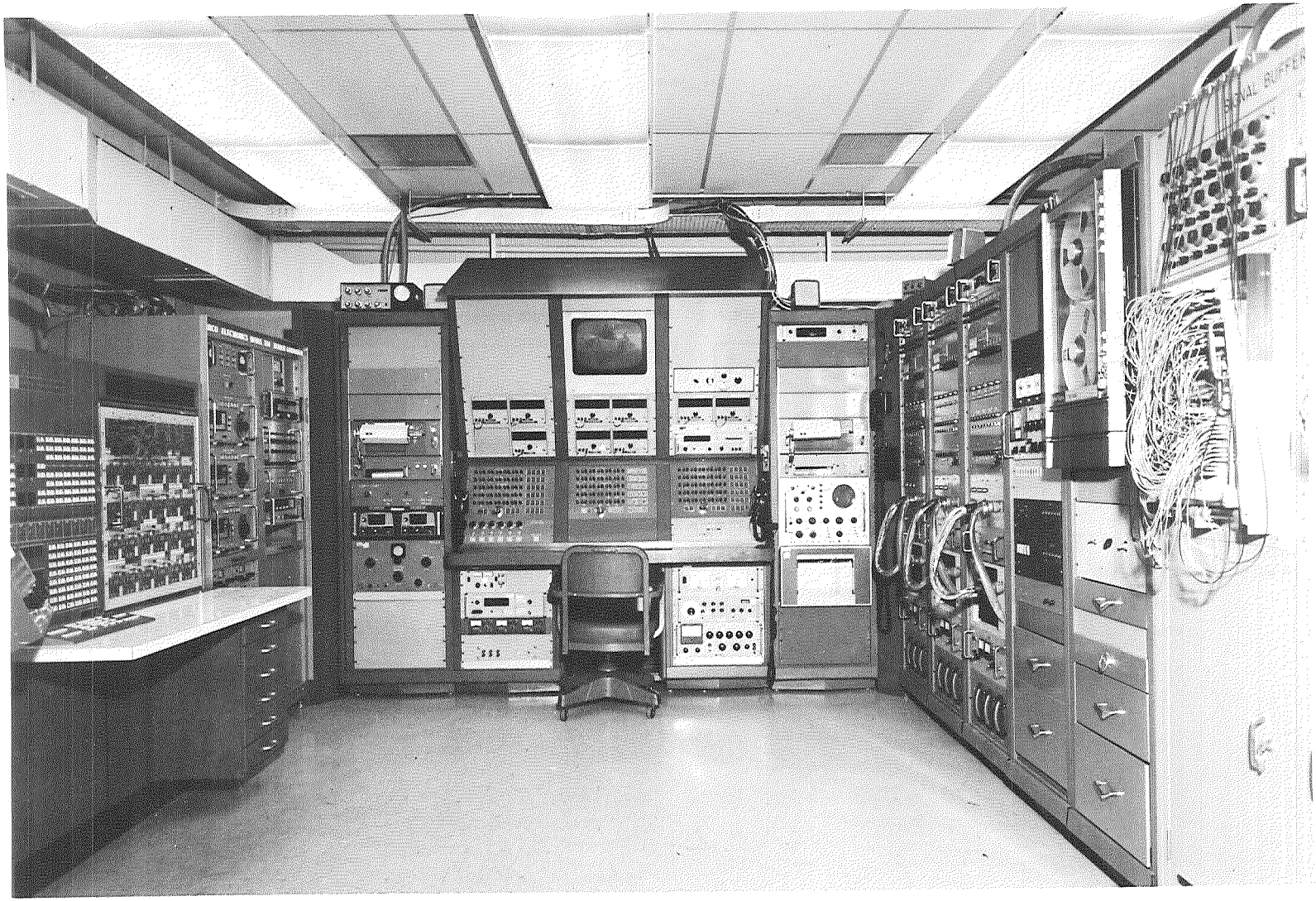

Figure 9.- Master-control room for CMG system. L-69-5141

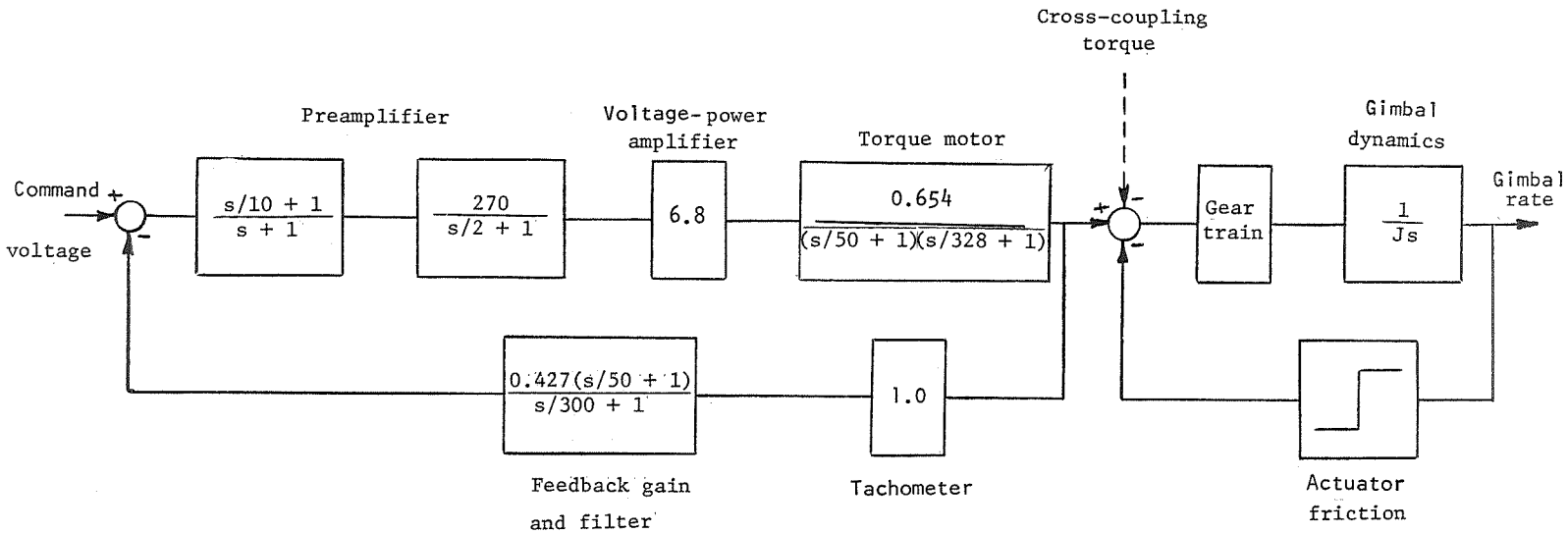

Figure 10.- Schematic drawing of CMG gimbal servo loop.

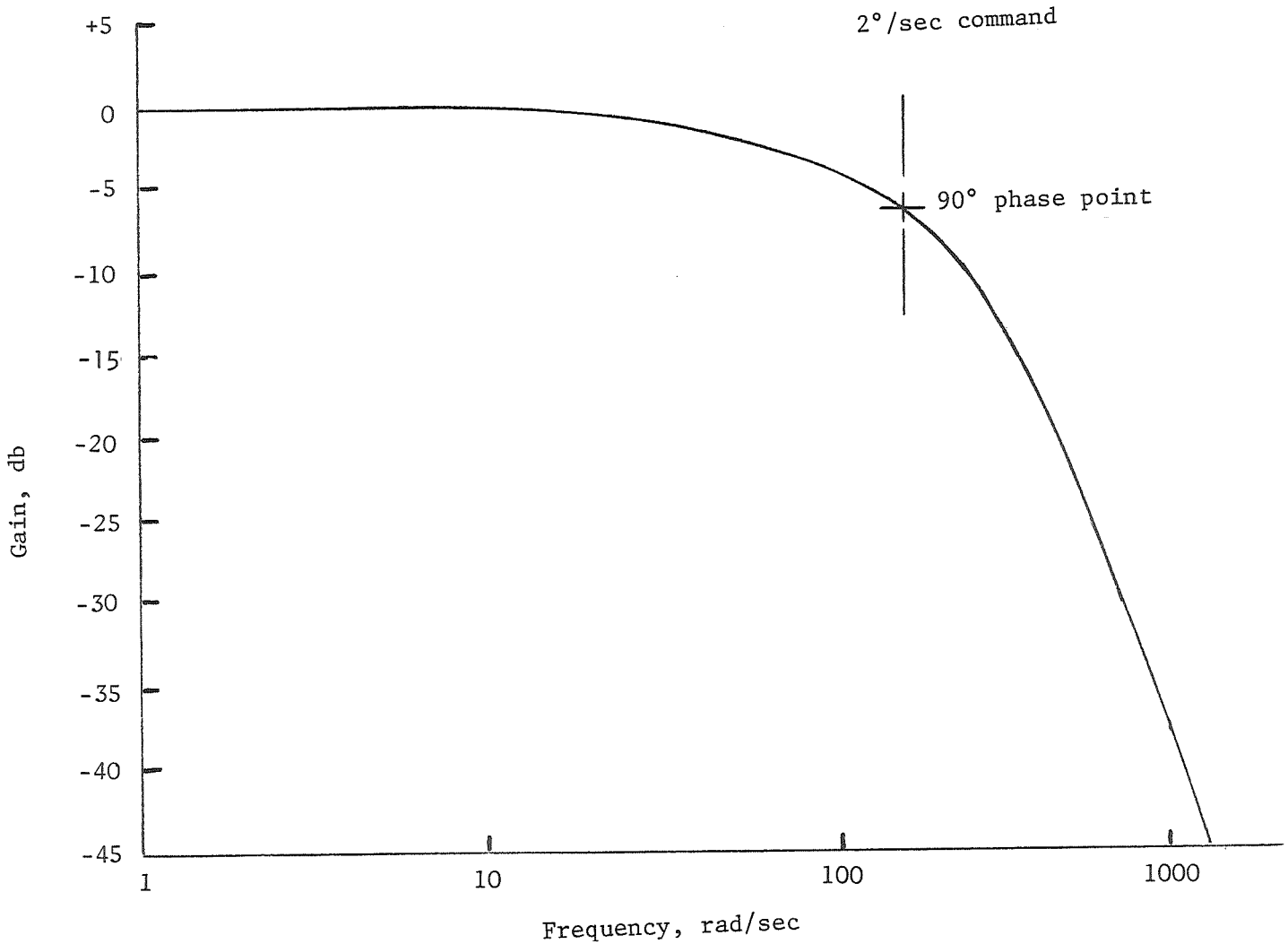

Figure 11.- CMG frequency response from motor tachometer.

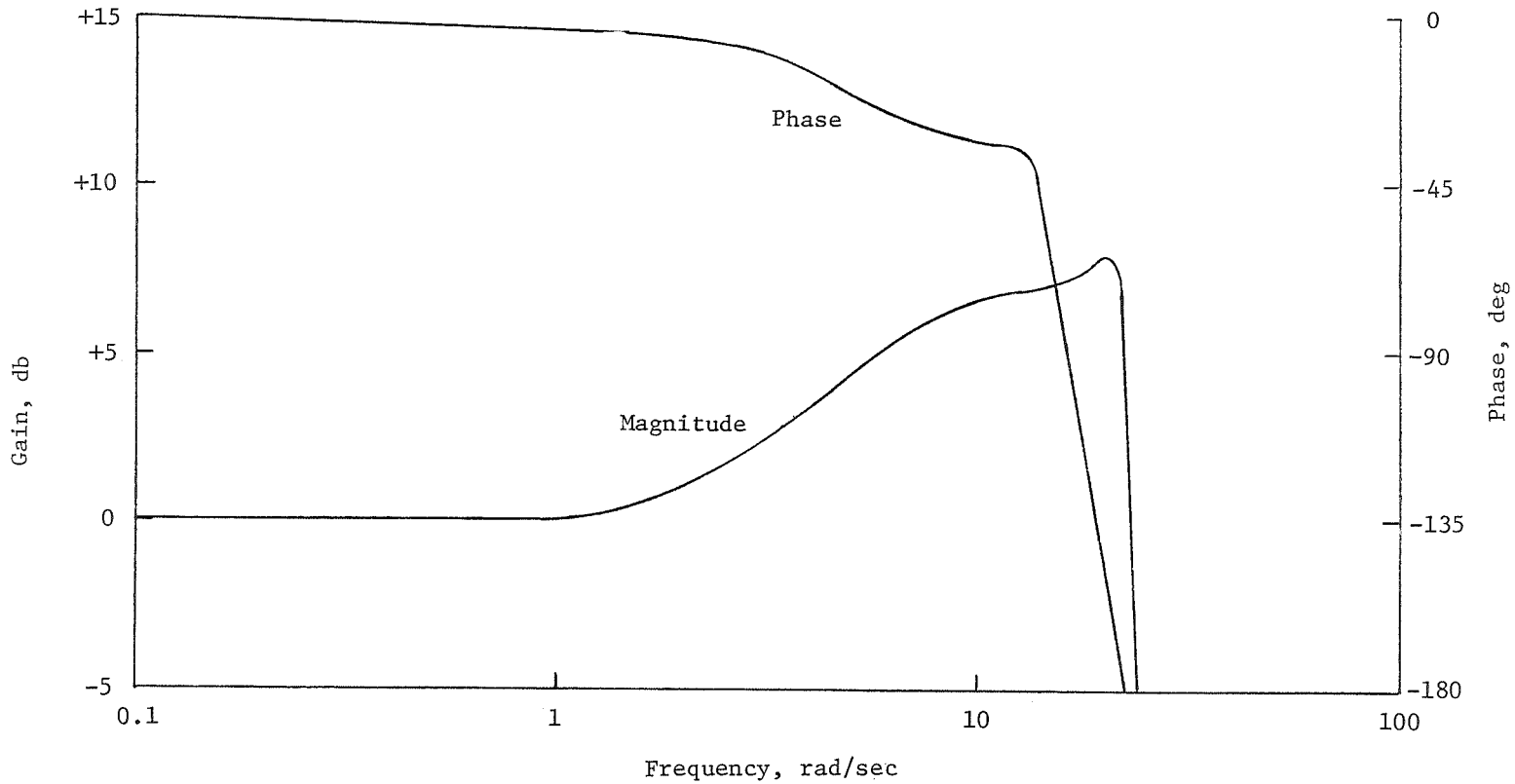

Figure 12.- CMG frequency response from gimbal tachometer.

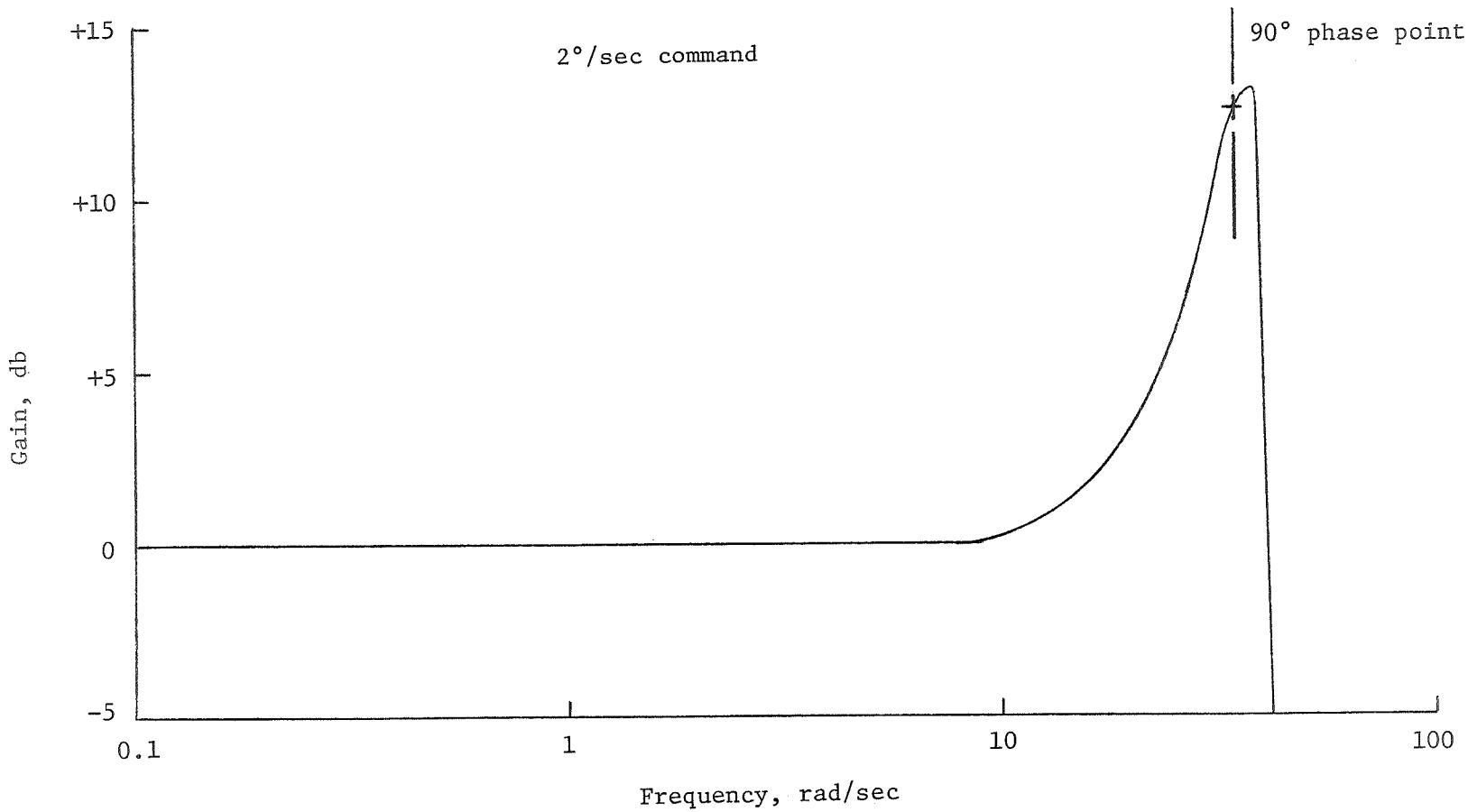

Figure 13.- CMG frequency response from gimbal tachometer with no cross coupling.

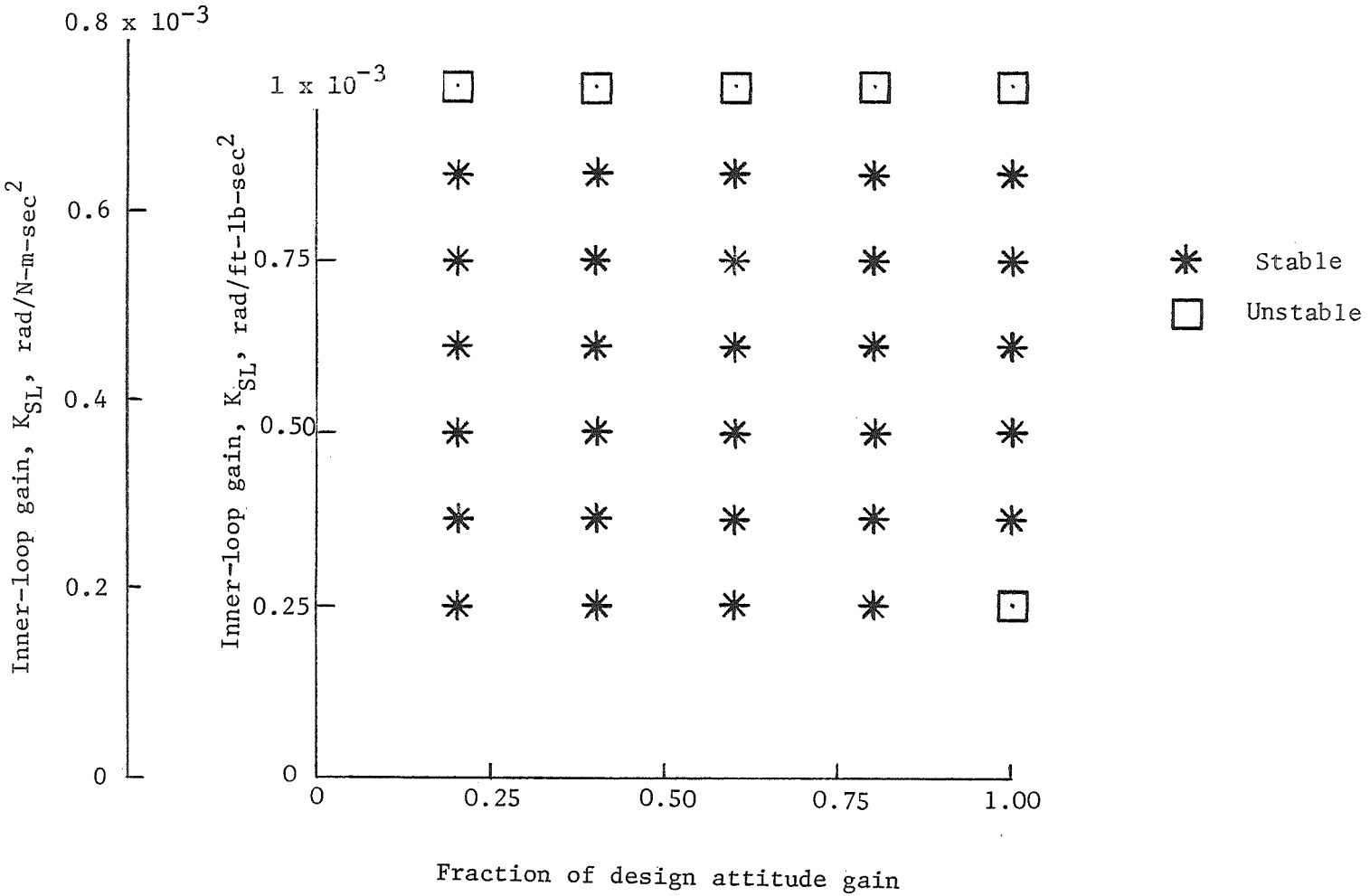

Figure 14.- System stability boundary. $\alpha = \beta = 0$.

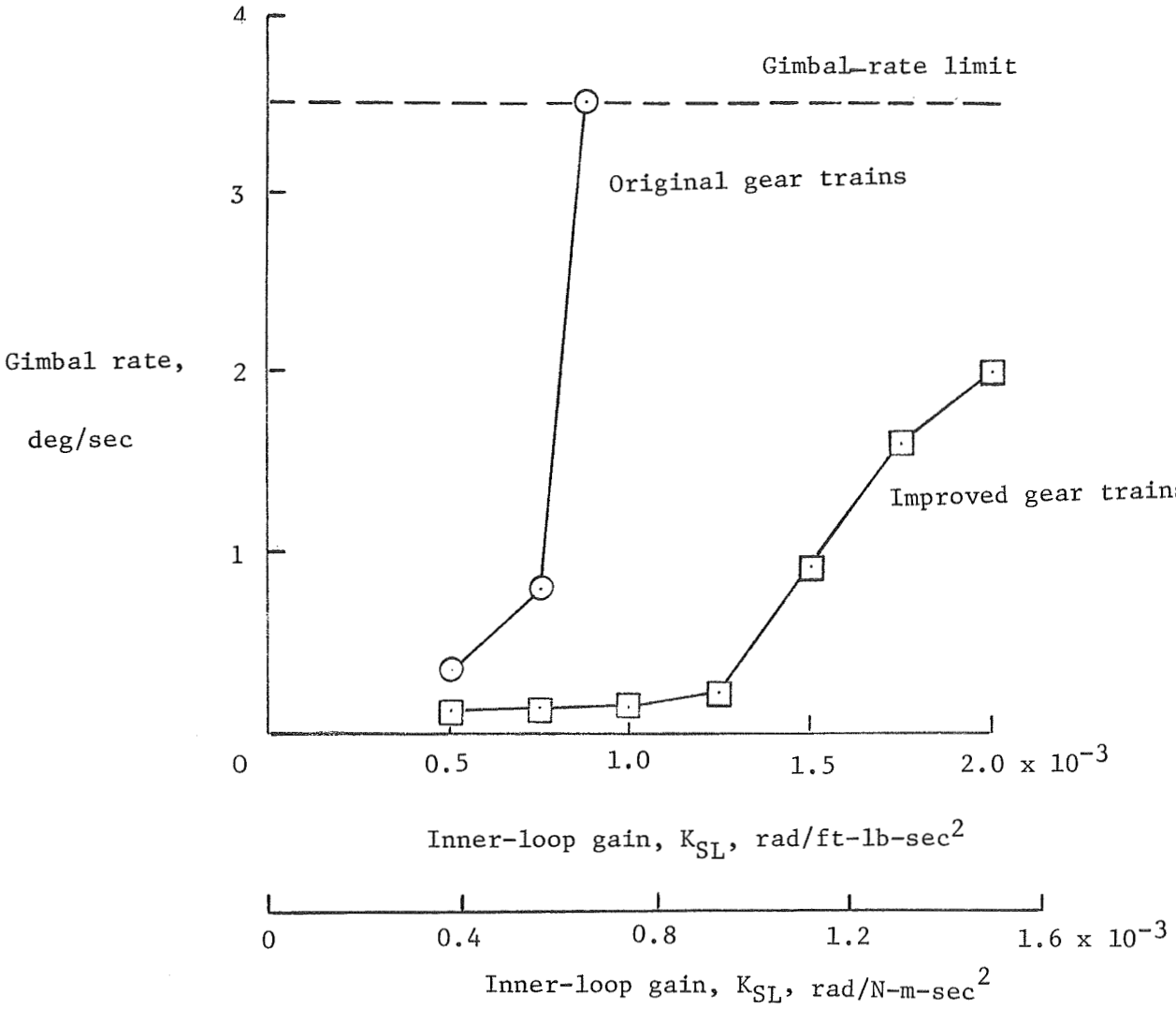

Figure 15.- Effect of gear-train modifications on hardware limit cycle.

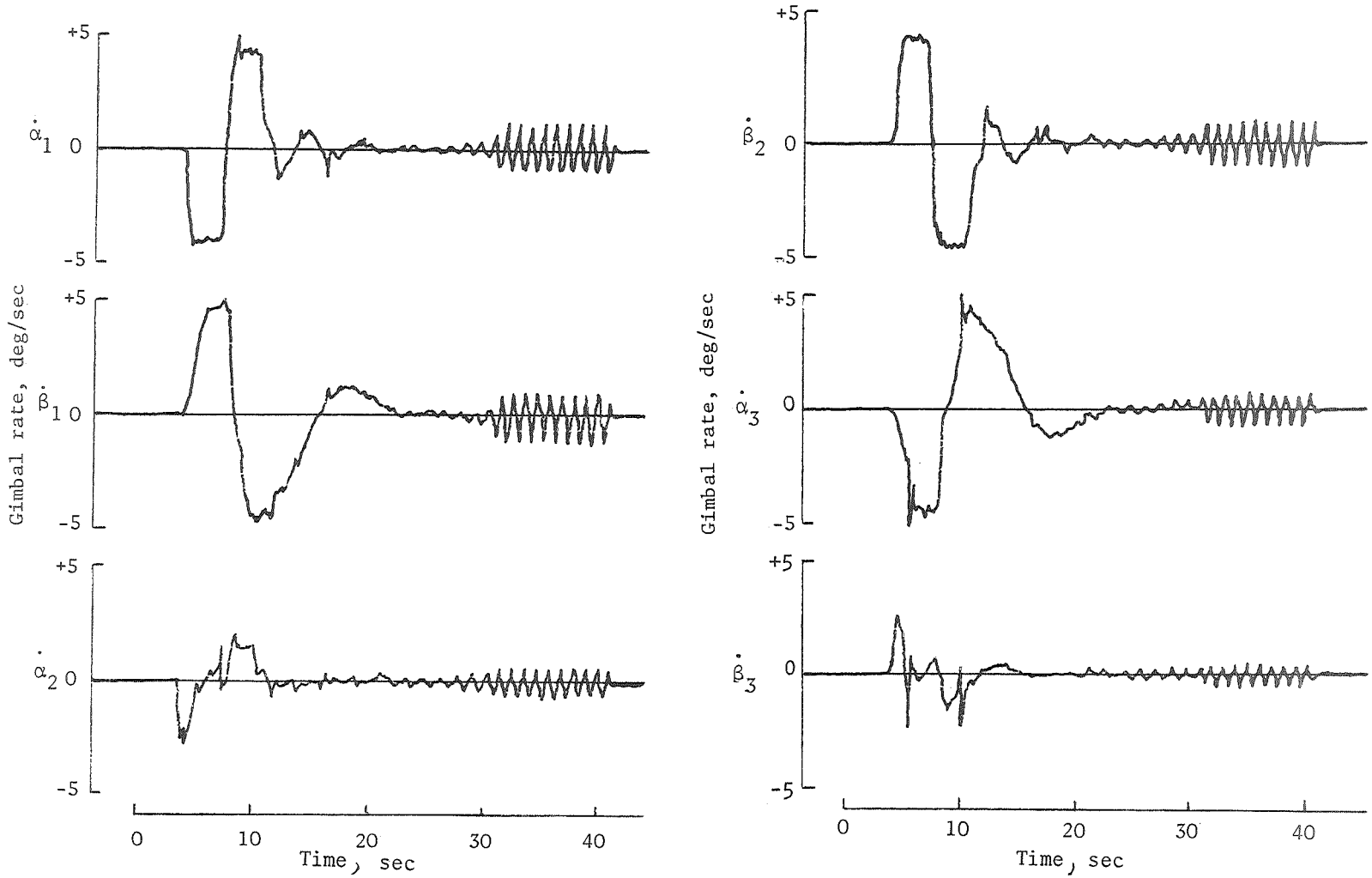

Figure 16.- System response with no position-feedback compensation.

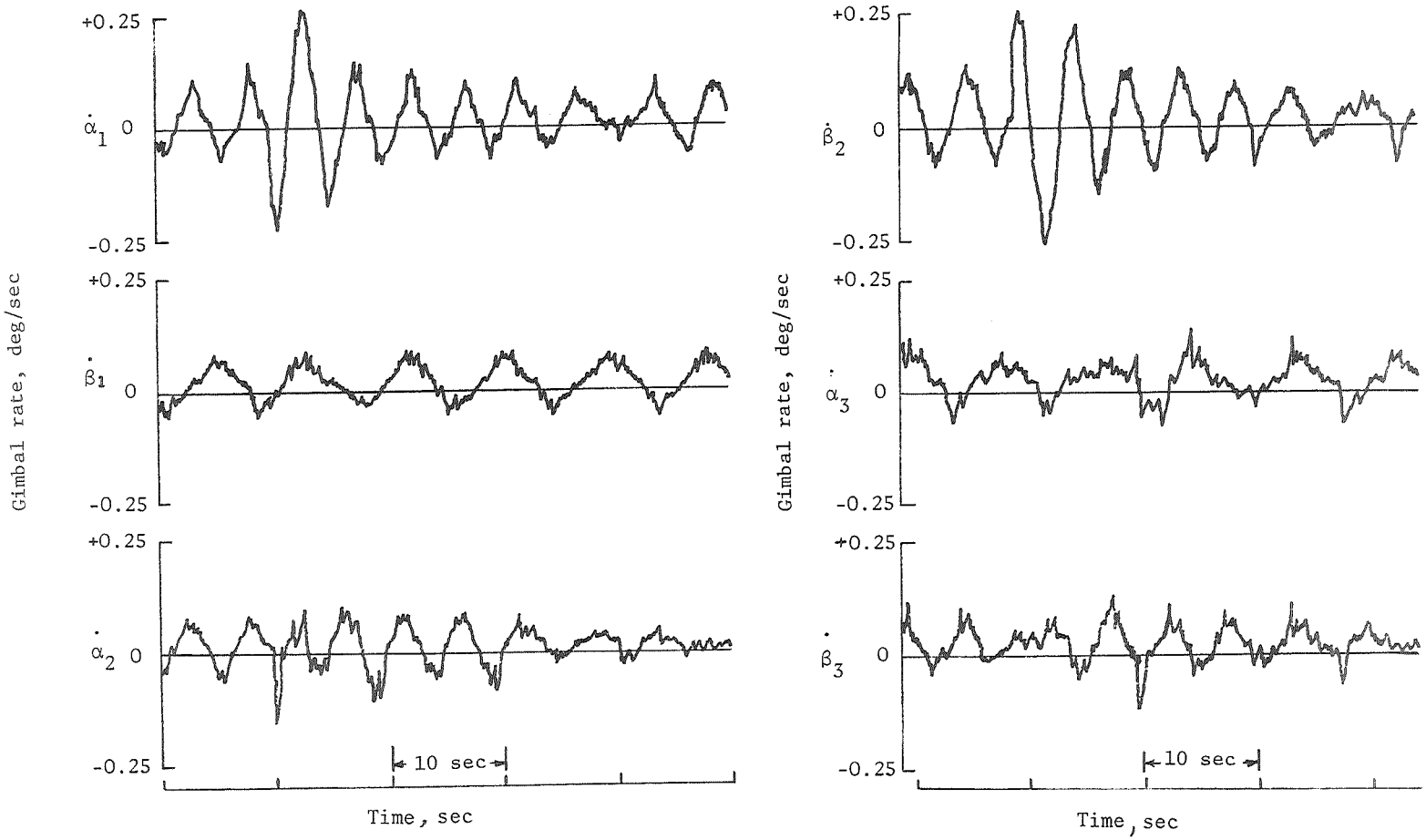

(a) K_a = 1.0 second.

Figure 17.- System response with position-feedback compensation.

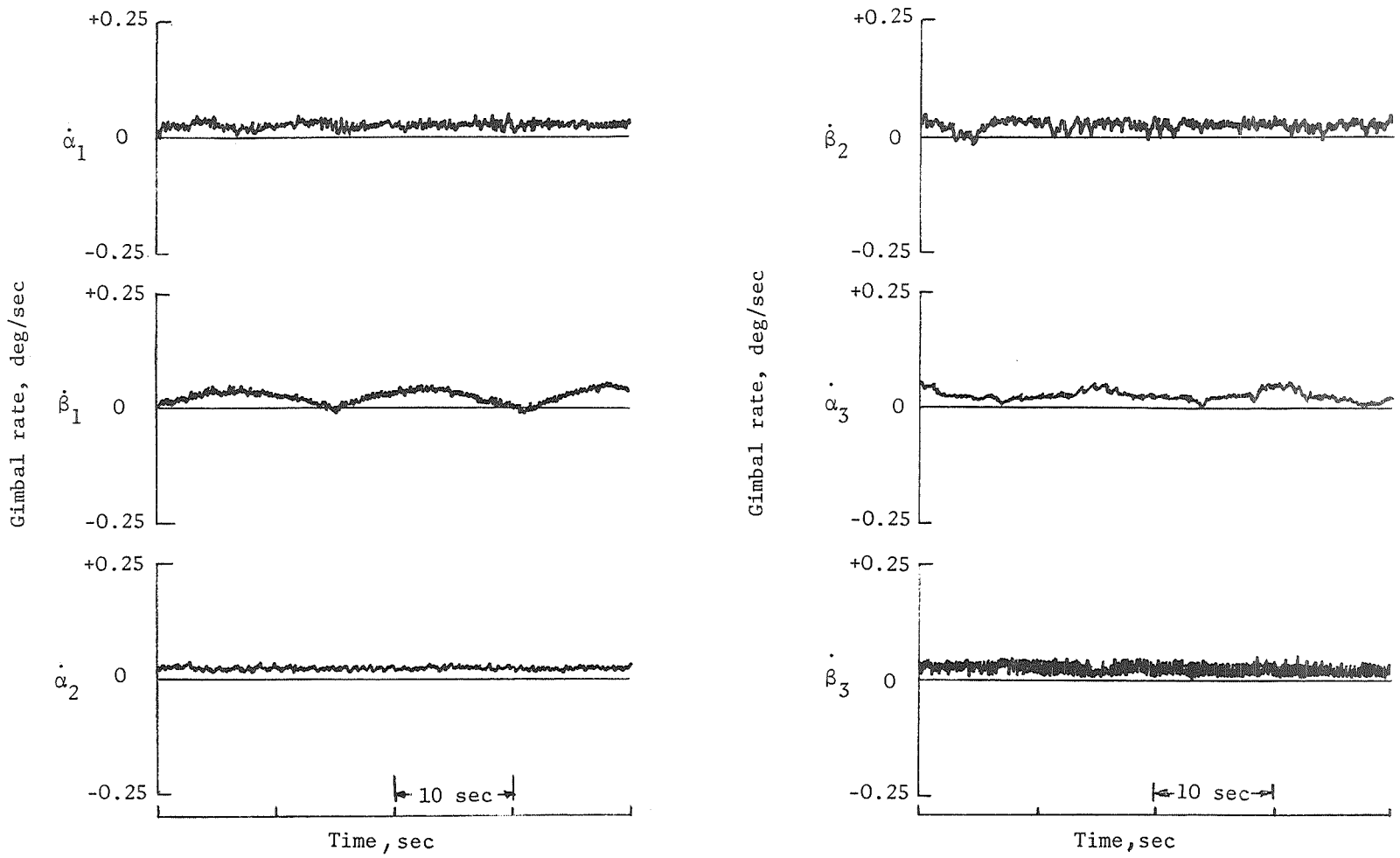

(b) K_a = 6.0 seconds.

Figure 17.- Concluded.

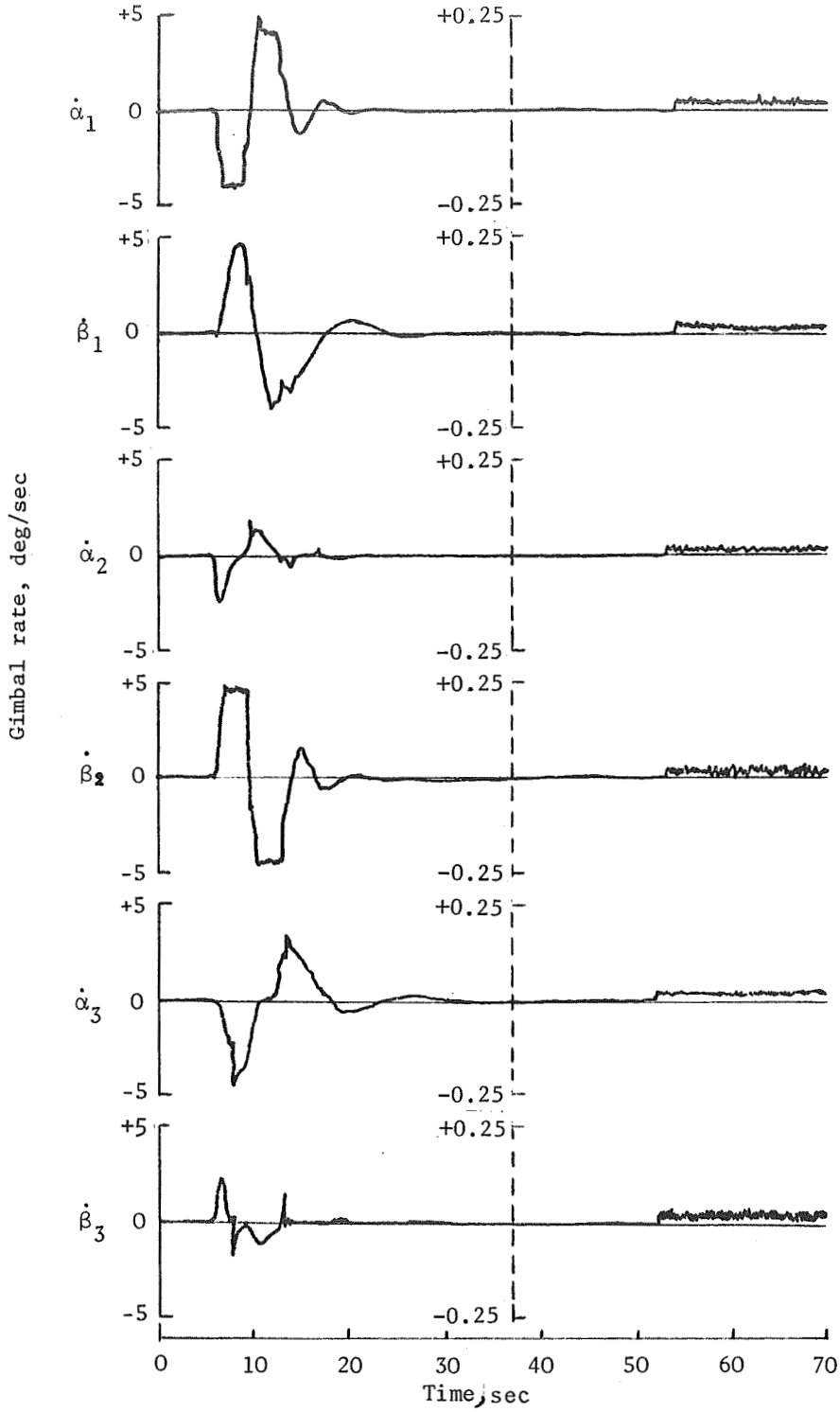

Figure 18.- System response to three-axis maneuver with position-feedback compensation for K_a = 16.0 seconds.

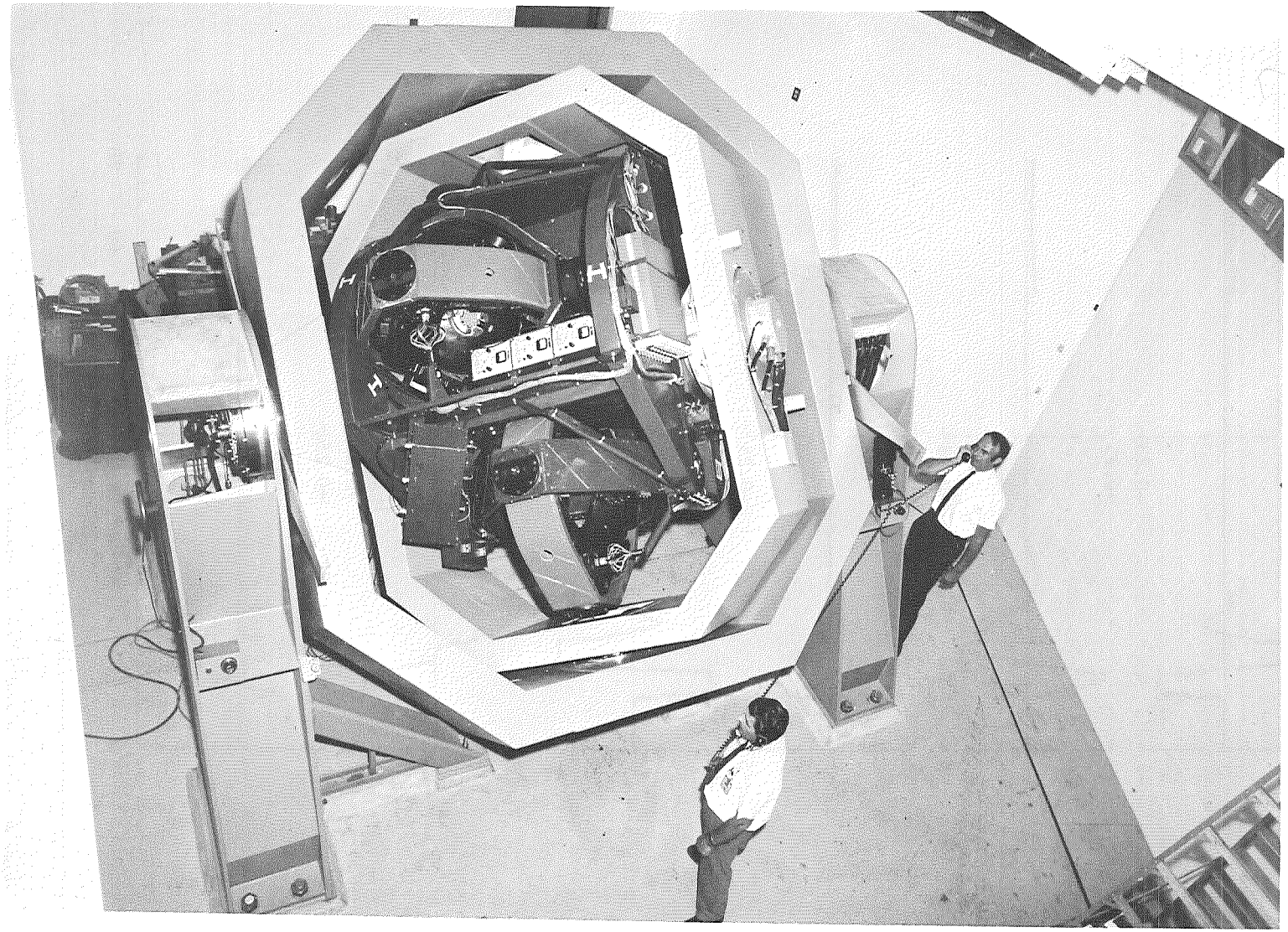

Figure 19.- CMG dynamic test setup. L-69-5142

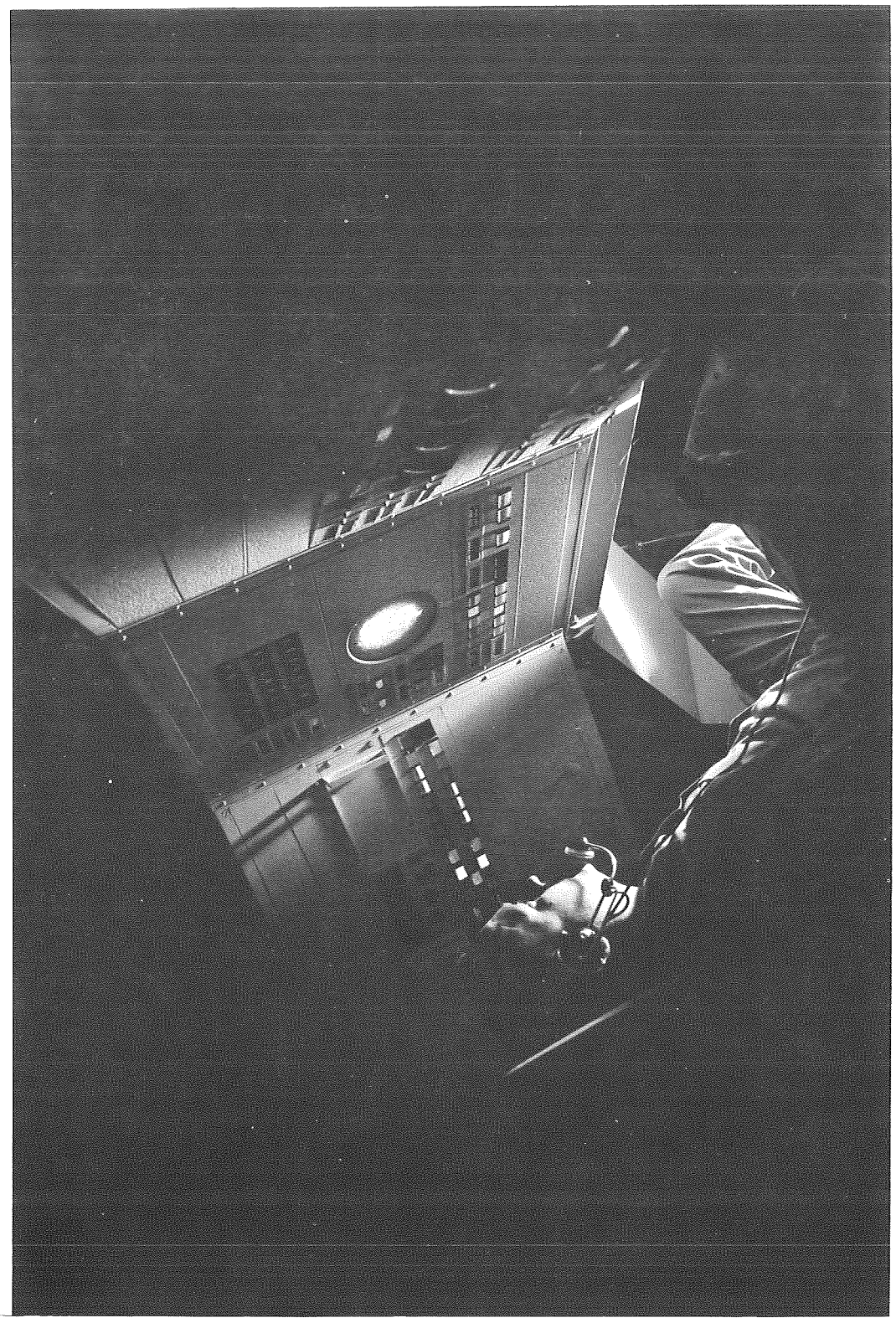

L-69-5437

Figure 20.- Pilot control console for CMG system.

NASA-Langley, 1970 —— 3 L-6555

NATIONAL AERONAUTICS AND SPACE ADMINISTRATION
WASHINGTON, D. C. 20546

OFFICIAL BUSINESS

FIRST CLASS MAIL

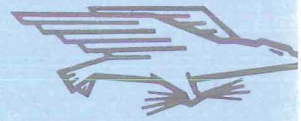

POSTAGE AND FEES PAID
NATIONAL AERONAUTICS AN
SPACE ADMINISTRATION

POSTMASTER: If Undeliverable (Section 158 Postal Manual) Do Not Retur

"The aeronautical and space activities of the United States shall be conducted so as to contribute . . . to the expansion of human knowledge of phenomena in the atmosphere and space. The Administration shall provide for the widest practicable and appropriate dissemination of information concerning its activities and the results thereof."

—NATIONAL AERONAUTICS AND SPACE ACT OF 1958

NASA SCIENTIFIC AND TECHNICAL PUBLICATIONS

TECHNICAL REPORTS: Scientific and technical information considered important, complete, and a lasting contribution to existing knowledge.

TECHNICAL NOTES: Information less broad in scope but nevertheless of importance as a contribution to existing knowledge.

TECHNICAL MEMORANDUMS: Information receiving limited distribution because of preliminary data, security classification, or other reasons.

CONTRACTOR REPORTS: Scientific and technical information generated under a NASA contract or grant and considered an important contribution to existing knowledge.

TECHNICAL TRANSLATIONS: Information published in a foreign language considered to merit NASA distribution in English.

SPECIAL PUBLICATIONS: Information derived from or of value to NASA activities. Publications include conference proceedings, monographs, data compilations, handbooks, sourcebooks, and special bibliographies.

TECHNOLOGY UTILIZATION PUBLICATIONS: Information on technology used by NASA that may be of particular interest in commercial and other non-aerospace applications. Publications include Tech Briefs, Technology Utilization Reports and Notes, and Technology Surveys.

Details on the availability of these publications may be obtained from:

SCIENTIFIC AND TECHNICAL INFORMATION DIVISION
NATIONAL AERONAUTICS AND SPACE ADMINISTRATION
Washington, D.C. 20546